(NASA-CR-157738) POST-SHOCK TEMPERATURES IN MINERALS (California Inst. of Tech.) 87 p HC A05/MF A01 CSCL 20B

N78-32897

Unclas
G3/76 31669

POST-SHOCK TEMPERATURES IN MINERALS

by

Susan A. Raikes *

and

Thomas J. Ahrens †

Seismological Laboratory
Division of Geological and Planetary Sciences
California Institute of Technology
Pasadena, California 91125

*Present address: Geophysikalisches Institut
Universität Karlsruhe
Hertzstrasse 16, Bau 42
7500 Karlsrutte-West (21)
W. Germany

†Correspondent

Abstract

An experimental technique has been developed for the measurement of post-shock temperatures in a wide variety of materials, including those of geophysical interest such as silicates. The technique uses an infra-red radiation detector to determine the brightness temperature of samples shocked to pressures in the range 5 to ∿30 GPa; in these experiments measurements have been made in two wavelength ranges (4.5 to 5.75μ; 7 to 14μ). Reproducible results, with the temperatures in the two wavelength bands generally in excellent agreement, have been obtained for aluminium-2024 (10.5 to 33 GPa; 125 to 260°C), stainless steel-304 (11.5 to 50 GPa; 80 to 350°C), crystalline quartz (5.0 to 21.5 GPa; 80 to 250°C), forsterite (7.5 to 28.0 GPa; ∿30 to 160°C) and Bamble bronzite (6.0 to 26.0 GPa; ∿30 to 225°C).

These results are generally much higher at low pressures (where they may even be in excess of the calculated shock temperatures) than the values calculated assuming a hydrodynamic rheology and isentropic release parallel to the Hugoniot but tend towards them at higher pressures. For example, in aluminium-2024, the theoretical post-shock temperatures, assuming a fluid-like rheology, are 35 to 218°C compared with measurements of 125 to 260° for the pressure range 10.5 to 33 GPa. However, the results are in considerably better agreement with values calculated assuming elasto-plastic behaviour (80 to 270°C) which probably also causes the high measured temperatures for stainless steel. In forsterite the measured values ranged from 65°C at 9.6 GPa (there was no detectable rise at 7.5 GPa) to 156° at 28.0 GPa, whereas the "hydrodynamic values" were 80 to 120°C. Values obtained for quartz were in excellent agreement

with those calculated by Mashimo et al. (1978) using release adiabat data: it is concluded the release path plays an important role in determining post-shock temperatures in silicates, and that release adiabat data should be used,wherever available, for calculations of residual temperatures.

Information obtained using this technique should place constraints on the thermal equation of state under shock conditions and have special relevance to the process of impact melting and planetary accretion.

Introduction

Shock wave equation of state data have long been used in the interpretation of impact metamorphism (e.g., Stoffler, 1971, 1972) and of density depth profiles of the earth obtained from seismic data (e.g., Al'tschuler, 1965). However, one of the limitations to these uses of Hugoniot data is the uncertainty in the temperatures reached both during the passage of the shock wave through the material and after unloading.

Shock temperatures have previously been calculated using Hugoniot data and the Mie-Grüneisen theory (e.g., Walsh and Christian, 1955; Wackerle, 1962; Ahrens et al, 1969; McQueen et al, 1970) which should yield reliable results for metals provided the rheology corresponds to fluid-like behaviour. However, the Mie-Grüneisen theory is inadequate over much of the pressure range for which shock wave data exist for silicates, since these all undergo major phase changes which may involve substantial changes in thermodynamic properties. Calculated Hugoniot temperatures can then be used to obtain post-shock temperatures assuming isentropic release. Unfortunately, there are few cases where there are sufficient data to either experimentally determine or theoretically calculate isentropic release paths; moreover the assumption of isentropic unloading from shock states has never been verified experimentally. Consequently, even if the Hugoniot temperatures were calculated correctly, large uncertainties could still exist in residual temperatures.

Calculations of post-shock temperatures in silicates, assuming release along isentropes lying above the Hugoniot, with the release volume greater that the initial volume, lead to values that appear too low to account for some of the effects seen in recovery experiments, such as the change in refractive

index observed in shocked silicate glasses (Gibbons, 1974). Where release adiabat data exist for silicates, they have been used in the calculation of post-shock temperatures (e.g. Gibbons and Ahrens, 1971; Ahrens and O'Keefe, 1972). This always leads to much higher, and possibly more credible, release temperatures (as is shown by the comparison in Table 1), largely because the release paths lie below the Hugoniot (Figure 1). However, no experimental tests of such calculations have been carried out for earth materials, and serious uncertainties exist in the post-shock temperatures of silicates of geophysical importance such as quartz and forsterite, even for material shocked to very modest pressure levels.

In view of the uncertainties that exist in the post-shock temperatures for silicates, their experimental measurement is important and could substantially increase the level of understanding of processes occurring under shock, as well as providing valuable constraints on the thermal equation of state at high pressures.

Early successful experiments designed to measure post-shock temperatures in explosively shocked metals by Taylor (1963) and King et al. (1967) were carried out with a photo-multiplier tube and InSb infra-red radiation detector respectively. Taylor's results for copper shocked to pressures in the range 90 to 170 GPa were in good agreement with the values calculated by McQueen and Marsh (1960) using the Mie-Grüneisen theory and fluid rheology. However, King et al. found large discrepancies between measurement and values based on these assumptions for copper at lower shock pressures, a result which was confirmed by Von Holle and Trimble (1976) for pressures less than 80 GPa. Some of the difference, especially at low pressures, may be explained by the contribution of elastic-plastic work (e.g., Foltz and Grace, 1969), and

the remainder may be due to non-hydrodynamic surface effects. These types of experiments were never really pursued because for moderate shock pressures in metals serious uncertainties in shock or post-shock temperatures did not appear to exist.

Experiments on non-metals have largely been limited to the determination of radiative properties of materials under extremely high pressures. Some attempts have been made to measure actual shock temperatures (Kormer, 1968) either photographically or photo-electrically, but these are limited to transparent materials where the radiation from the shock front may be observed as it propagates through the material, eliminating the necessity of having a detector with a rise time similar to that of the shock wave. In particular, optical measurements in the visible region have been used to investigate the melting curve for alkali halides under pressures in the range 50 to 300 GPa (Kormer et al., 1965).

However, no attempts were made to expand the scope of the early experiments, such as those of Taylor and King et al., to include the measurement of post-shock temperatures in non-metals, even though large uncertainties exist for silicates. This was largely because the supposedly lower temperatures, coupled with the low sensitivity of available detectors, meant that experiments such as those of King et al. were not feasible. Recent improvements in detector technology have now made it possible to design a system capable of measuring post-shock temperatures in silicates; the availability of such data should help resolve the current uncertainties.

Experimental Technique

Initial experiments were designed with the aim of investigating residual temperatures in silicates of geophysical interest shocked to pressures up to 30 GPa. The materials chosen were crystal quartz, Bamble bronzite (both of which undergo phase changes in this pressure range) and forsterite; for completeness, the materials used as driver plates in the experiments, namely aluminium-2024 and stainless steel-304, were also studied.

The method developed for experimental determination of post-shock temperatures involves the monitoring of radiation from the back (free) surface of a shocked sample with an infra-red radiation detector whose output may then be used to determine the brightness temperature of the sample. Since the residual temperatures for the pressure range to be investigated were expected to be of the order of 400°K, and the Planck distribution law gives a maximum in spectral radiance between 3 and 9 μ for black bodies radiating at temperatures from 1000 to 300°K (Touloukian and DeWitt, 1972) infra-red detectors were a logical choice for this study. In addition, since silicates behave as fairly good black bodies in the infra-red beyond ∿5μ, with the exception of the silicate absorption band at ∿9μ, the radiative output of the sample is also maximised. A schematic plan of the experimental lay-out is shown in Figure 2.

a. Production of the shocked state

In these experiments, the shocked state was produced in the sample by the impact of a gun launched flyer plate. The technique is described in detail in Gibbons (1974), and has been used by a number of authors (e.g., Ahrens et al., 1971; Ahrens and Gaffney, 1971; King and Ahrens, 1976).

The gun used is a propellant gun with a barrel ∿ 3.3m long and a ∿ 20mm bore; it is capable of accelerating a typical projectile, bearing an aluminium, steel or tungsten flyer plate, to speeds up to ∿ 2.5 km/s. The velocity is determined by the amount of powder used; there is a good linear correlation between the ratio of powder charge to projectile mass and velocity which allows the velocity, and hence the pressure, to be pre-determined. The actual projectile velocity is determined by measuring the time interval between obscurations (by the front of the projectile) of two laser beams located 10.5 and 4.5 cm from the muzzle of the gun. The shock pressure reached in the sample may then be calculated using the impedance match method (e.g., Duvall and Fowles, 1963) and the known Hugoniots of flyer plate, driver plate and sample materials.

The accuracy of the pressure calculation depends on the precision of the velocity measurement and of the Hugoniot. In fact, the uncertainties in velocity, typically ±0.05 km/s are probably small compared with the scatter in the measured equation of state points, at least for natural materials such as crystalline quartz and Bamble bronzite, especially at pressures close to the Hugoniot elastic limit which can vary from sample to sample, and to phase transitions. A likely estimate of the uncertainty in pressure would be ±0.5 GPa in the metals and ±0.5 to 1 GPa in the other materials studied.

After passing through the mylar window sealing the end of the barrel, the projectile makes contact across a shorting target and finally impacts the target assembly, (Figure 2). In order to achieve nearly one-dimensional planar flow upon impact of the projectile with the target, the target is carefully aligned using the normal reflection from the target surface of a laser beam shining down the centre of the barrel. The target assembly consists of a driver plate (1.5mm aluminium-2024 or stainless steel-304), and a 3mm thick silicate sample, 15mm in diameter, mounted on it by epoxy

around the edges. In the case of shots on metals, the driver plate, now 3mm thick, is the sample.

b. Temperature measurement

The brightness temperature of the back (free) surface of the sample is determined from the output from an infra-red detector. This detector is mounted above the impact chamber (Figure 2), and monitors the back face of the sample via a mirror and optical system. The latter ensures that only the centre (~0.8 cm dia) of the sample is viewed, reducing the contribution from edge effects (also somewhat lessened by using a circular sample) and increases the efficiency of the detection system. The detector is connected via an amplifier to two oscilloscopes. One is triggered by the passage of the projectile past the first laser beam of the timing system, and records the detector output at a rate of 50 μs/div. This provides a back-up record in case of failure of the higher time-resolution recording, and a means of checking that no temperature signals are generated prior to the passage of the shock wave through the sample assembly. (Note that it also provides another means of determining the projectile velocity.) The second oscilloscope is triggered by the contact of the flyer plate with the shorting target, which is approximately 15 mm in front of the driver plate, just prior to impact; this writes at 5 μs/div, and it is the primary record that is used in temperature determination. A typical record shows a sharp rise in signal corresponding to the arrival of the shock wave at the free surface of the sample, followed by a level portion corresponding to the residual temperature, and then a subsequent rise due to air shocks generated at the end of the sample chamber and the destruction of the mirror. Actual records will be discussed in detail in the next section.

The detectors used in these experiments were InSb and HgCdTe, which are operated at 77°K and are enclosed in dewars cooled by liquid nitrogen; both were obtained from the Santa Barbara Research Centre (Goleta, California) and typical response curves, obtained from S.B.R.C., are shown in Figure 3. Additional operational details are listed in Appendix A. A filter was used to limit the bandwidth of the InSb detector to 4.5 to 5.75μ in order to minimise the possibility of radiation from the metal driver plate, or metal-sample interface, being transmitted through the sample and causing errors in the temperature determination. (As can be seen from the transmission scans of Figure 4, which were obtained using a Perkin-Elmer Model 180 Infra-red Spectro-photometer in a manner analogous to that described in Burns (1970), this is unlikely to be a problem for quartz or bronzite but the forsterite does transmit significantly up to 5μ.)

The InSb detector was used with a variable gain amplifier (Raikes, 1978); the system rise time, which is essentially limited to $\sim$0.2 μs by the chip itself, was $\lesssim$0.5 μs depending on the gain setting used. Although the HgCdTe is a faster material ($\lesssim$0.1μs), the rise time of the detector-amplifier system was $\lesssim$0.8 μs because an electronic filter with a high frequency cut-off of 5MHz had to be used to reduce the large amount of high frequency noise which would otherwise have made accurate measurement of temperature impossible.

In order to convert the voltage record into a brightness temperature, the detector must be calibrated. This is best performed by heating the sample *in situ* to a known temperature, and recording the corresponding voltage output of the detector-amplifier system. This is easily done for metals, but would be very hard for the non-metals studied since they are extremely brittle and hard to heat in the experimental configuration without cracking. Instead, advantage was taken of the fact that they behave as fairly good black bodies beyond $\sim$4.5μ, with the exception of the

silicate absorption band at $\sim 9\mu$, and a calibration curve obtained for a "black" body (graphite), corrections for emissivity were estimated from available data, as described below.

Typical calibration curves are plotted in Figures 5 and 6, and Table 2 gives the power law fits to the curves. Both detectors gave extremely reproducible calibration curves, as is demonstrated by the two sets of points for aluminium in the case of InSb (these were obtained several weeks apart with a number of shots fired in between).

Souces of error.

Errors in temperature measurement can basically arise from two causes -- those related to the sample, and those originating from outside sources. Prime among the latter is contamination of the signal by radiation from air shocks which can be of extremely high temperature. Owing to the geometry of the apparatus these should not be important prior to the arrival of the shock wave at the free surface of the sample, and, indeed, no earlier signal rises were detected. The only air shock likely to affect the post-shock temperature measurement would be one generated at the back of the sample itself, which is (hopefully) eliminated by the sample vacuum chamber that is pumped down to $\lesssim 5\mu$. To reduce further possible radiation from residual gases within this chamber heated by compression due to the shock wave, the chamber was flushed out with helium prior to each shot. Radiation from later air shocks, such as that generated at the end of the sample chamber as the window breaks, is clearly visible on each record, and ultimately causes the detection system to saturate. If the samples were transparent, then radiation from the metal driver plate could add to the signal, but the rise should then precede the free surface arrival of the shock wave, and this does not in general appear to be the case. Anyway,

the emissivity of the metal is substantially lower than that of the sample, so this effect should be relatively small, and both detectors were chosen to operate at wavelengths where the samples are nearly opaque. (Forsterite does have a 20% transmittance at 4.5μ dropping rapidly to less than 5% at 5μ, and so may show minor effects due to transmitted radiation for the InSb detector.) Both the driver plate and the sample surface in contact with it were polished prior to mounting of the sample in order to minimise the "porous" surface interactions that could give rise to considerable heating (see e.g., Urtiew and Grover, 1974); this also reduces the likelihood of air being trapped in this interface, but this should be removed by the evacuation of the sample chamber. In order for the signal to be contaminated by radiation from the metal or the driver-sample interface, large changes must take place in the transmissivity of the sample under shock conditions; although changes have been reported in sapphire (Urtiew, 1974), these were decreases and at much higher pressures. It seems that this is not a likely source of error. Vibration of the detector-amplifier system could conceivably affect the output. However, the detection system was physically clamped in isolation from the gun, and vibrational effects were not apparent except for some HgCdTe shots where a negative signal of short duration (∿10 μs), obviously non-thermal in origin, was observed prior to impact with the shorting target, but the output returned to the zero level before the free surface arrival.

Two main sources of errors associated with the sample behaviour under shock are changes in emissivity and the effects of non-uniform heating. The former may be investigated by comparing the brightness temperatures obtained at different wavelengths, since the change would probably not be constant as a function of wavelength. Changes in emissivity may be related to phase changes, changes in surface properties and triboluminescence.

In a recent work on residual temperatures in copper, Von Holle and Trimble (1976) determined temperatures by using the ratio of detector signals obtained at different wavelengths. They believed this would reduce the likelihood of error due to changes in emissivity and the effects of surface processes, and yield a relatively unbiassed estimate of the post-shock temperature. Unfortunately, for materials in which the emissivity is not a strong function of wavelength, such as stainless steel and aluminium,small errors in measurement of the detector output can lead to large changes in the ratio of the signals from the two detectors and totally unreasonable ratio temperatures, so that this technique has not proved useful.

The effects of non-uniform heating may be more severe; they were estimated by calculating the temperature that would be measured if 10% of the surface were 100 or 200°K hotter than the remaining 90%. For a 100° excess, the discrepancy between "measured" and mean temperatures is close to the accuracy of measurement, i.e.$\sim\pm$10°. However, for a 200° excess the differences may reach $\sim$30° (with the measured temperature being an over-estimate), although such a temperature distribution seems rather unlikely because of the energy partition that would be required. The effect of surface processes such as jetting can also bias the temperature measurements; these will presumably be more important in metals where the optical depth is of the order of angstroms, than in silicates where it is microns. To reduce the likelihood of jetting, the sample surfaces were polished, but not to a high gloss as this would reduce the emissivity.

Observations

Typical detector output records are shown in Figures 7-9; in all cases, the interpretation of the voltage output is based on the assumption that the oscilloscope sweep at 5 μs/div is triggered at the moment of contact

of the flyer plate with the shorting target (see Figure 1). This was checked both by analysing the timing of the signals seen on the back-up record triggered by the passage of the projectile past the first laser beam, and by using a delayed trigger on the oscilloscope. The assumption appears valid to within $\sim\pm 0.5$ μs, which is close to the rise time of the detector.

a) Stainless Steel-304 and Aluminium-2024

Typical detector output records are shown in Figure 7: these are for the InSb detector, but the records obtained with the HgCdTe detector were essentially similar except for the longer rise time; the records were extremely reproducible. In general, the output shows a sharp, but low amplitude, rise corresponding to the free surface shock arrival, followed by a short level portion taken to correspond to the residual temperature. This is followed by a rapid rise to a peak occurring ~ 7 μs after the free surface arrival, and subsequently the detector-amplifier system saturates upon arrival of radiation from an air shock generated at the end of the sample chamber. At the highest pressures, the separation of the initial level portion and the rise to the peak was indistinct; in these cases, the post-shock temperatures were determined from the output level 0.5 μs (InSb) or 0.75 μs (HgCdTe) after the free surface arrival. (These values correspond to the rise times of the detection systems.) In the shots using the HgCdTe detector, the system saturated prior to the arrival of radiation from the air shock, and the peak temperatures could not be determined.

The temperatures determined in this manner are listed in Tables 3 and 4; in general, the agreement between the values for the two wavelength ranges is good, with the difference not exceeding the estimated uncertainty in the measurement. The values of post-shock temperatures

in stainless steel 304 were found to vary from 80°C at 11.5 GPa to 355°C at 50 GPa; these values may be compared with those calculated by McQueen et al. (1970) which ranged from 25 to 175°C. In aluminium-2024 the measured values went from 125°C at 10.5 GPa to 260°C at 33 GPa; the corresponding theoretical values are 35 to 218°C (McQueen et al., 1970). The values for steel may at first seem high when compared to the small amount of heating apparently observed in steel containers used in recovery experiments; however, these containers are not examined immediately, and the initial post-shock temperatures will quickly decay owing to thermal conduction. This is borne out by the observations of Schneider and Stilp (1977) who used thermocouples to measure the temperature within large steel targets as a function of time and distance from the centre of impact. The time resolution of their measurements was only 50 ms, and they found that the temperature decayed rapidly as a function both of time and of distance away from the impact. Since in the current experiments the temperature at the centre of impact is observed within 1 μs of the shock wave arriving at the free surface, the high observed temperatures are not inconsistent with the maximum increase of 18°C observed 1.2 cm from the impact centre by Schneider and Stilp.

The origin of the later peak, whose temperature could only be determined for the InSb experiments, is unclear, but it appears to be a material property rather than some effect common to all shots such as the compression of residual gas within the sample chamber. It correlates well with pressure, shock, and free surface velocities for both stainless steel and aluminium, but the curves are separate for the two materials even if the temperature is estimated using the same calibration curve. It may be due to some form of localised frictional heating on break-up of the sample.

Discrepancies between measured and (hydrodynamically) calculated temperatures have also been reported for other metals by several authors (e.g., Von Holle and Trimble, 1976); however, sources of error that might produce them should be considered. Since the optical depth is only angstroms, the behaviour of the surface layer is important: heating within this layer, such as discussed by Urtiew and Grover (1974), may lead to high temperatures unrepresentative of the bulk sample, especially if the heating is non-uniform. The surface is also an important factor controlling the emissivity, and roughening of the surface by the passage of the shock wave through it, and by such processes as jetting, could cause an increase in emissivity leading to an over-estimate of the temperature. For this reason, the corresponding black body temperatures, which are lower bounds on the residual temperatures, are also tabulated in Tables 3 and 4. They are still in excess of the calculated values for stainless steel, but are lower than the theoretical values for aluminium, which is not surprising as in the latter case the black body temperatures represent a five-fold increase in emissivity, which is highly unlikely (a two-fold increase would yield temperatures in the range 90 to 260°C). The consistency of the results for the two wavelength ranges suggests that the high observed temperatures are real; the implications of this will be discussed later.

From these experiments it appears that, in view of the low emissivity of the metals, the small signal corresponding to the post-shock temperature, and the low transmission coefficients of the silicate samples in the wavelength range studied, there should be no significant contribution to the temperatures measured for the silicates due to radiation from the driver plate.

b) Silicates

Typical oscilloscope records for the silicates studied (natural single crystal quartz, cut perpendicular to the c axis; synthetic single crystal forsterite, cut perpendicular to the c axis; Bamble bronzite) are shown in Figures 8 and 9; once again they were extremely reproducible. Initial estimates of post-shock temperatures were based on the assumption that they behaved as black bodies in the wavelength range studied. For quartz in the range 5 to 8μ this is a reasonable approximation since the emissivity is greater than 0.9 (Touloukian and DeWitt, 1972), and is probably justified for the Bamble bronzite in the InSb range, since it does not transmit. However, the forsterite has a 20% transmittance at 4.5μ (dropping rapidly to less than 5% at 5μ), and the presence of the silicate absorption band at ∿9μ can cause a large drop in the emissivity. The latter effect is clearly visible in the comparison of black body and quartz emittance spectra at temperatures from 250 to 500°K presented by Lyon (1965).

Emmissivities of silicate materials have been studied largely with the objective of interpreting observed emission from the terrestrial planets in terms of their surface composition, and are thus available largely for rocks and powdered samples. In order to estimate the probable effect of the emissivity on the post-shock temperatures obtained, the values of the emissivity for quartz and dunite (primarily forsterite) given by Buettner and Kern (1965), Lyon (1965) and Touloukian and DeWitt (1972) were used to calculate correction factors as follows:

The detector output S for an operating wavelength range from λ_1 to λ_2 may be expressed as

$$S = \int_{\lambda_1}^{\lambda_2} E(\lambda,T)D(\lambda)P(\lambda,T)d\lambda \qquad (1)$$

where $E = (\lambda,T) = E(\lambda)$ = emissivity (assumed independent of T)

$D(\lambda)$ = detector response, $P(\lambda,T)$ = Planck's function

λ = wavelength, T = absolute temperature.

This may be integrated numerically and used to derive the ratio of the signal obtained for a silicate at temperature T to that for a black body at the same temperature. The correction factors are listed in Table 5 the values for bronzite were estimated from its absorption spectrum which has a broad peak between 8.5 and 12.5μ although the maximum absorption does not exceed 55%; in quartz the peak absorption, at ∿9.0μ, is almost 80%. (The effect of surface roughness is to change the contrast between the emissivity minimum at the absorption peak and the maximum; the latter value varies little with surface finish.)

Since the post-shock temperatures are measured after the interaction of the shock-wave with the free surface, and that interaction will cause roughening of the surface, a correction factor derived for a rough surface might be more appropriate; however, the values listed in Table 5 for polished surfaces will be used since these should yield an upper bound on the temperature. Two additional factors should be taken into account: one is that the absorption peak may shift during shock compression (e.g., Goto et al., 1977), and broadening of the absorption bands for SiO_2 has been observed in samples recovered after shock compression to pressures up to 52 GPa (Mashimo et al., 1978). The second is the possibility of triboluminescence, or some other form of non-equilibrium radiation such as might be associated with a phase change; in these cases the emissivity may even exceed unity. Because of these uncertainties, the black body temperatures may well be more reasonable estimates of the residual values and will be used later in a comparison of observed and calculated temperatures.

The corrected values of Tables 6-8 probably represent upper bounds to the post-shock temperatures.

Quartz

The signals recorded using the InSb and HgCdTe detectors are extremely similar for quartz; the main features are a "flash" of short duration, which occurs at (or near) the time of arrival of the shock wave at the free surface, a subsequent drop to a level "trough" (taken to represent the post-shock temperature) followed by a rise and eventual saturation due to radiation from air-shocks. At pressures below about 15 GPa the level portion after the initial peak is well defined, and it is this that is used to determine the residual temperature; however, at higher pressures the later "arrivals" tend to mask this, and the temperatures measured will in general be overestimates. (This is especially true for the slower HgCdTe detector, and probably accounts for the high measured temperature at 19.5 GPa.)

Temperatures determined for various shock pressures are listed in Table 6; with the exception of the 19.5 GPa shot the residual values (both black body and corrected) are in quite good agreement for the two wavelength ranges, although the peak values are rather different. There appears to be a slight break in slope after the initiation of the phase change (at ~14 GPa). One interesting feature is that quite high post-shock temperatures were measured for pressures below the Hugoniot elastic limit, which is 6.5 to 8.0 GPa (Wackerle, 1962); this observation is rather surprising since the elastic compression would be expected to be reversible.

The initial flash might be explained in a number of ways. If it only occurred for the InSb shots, it might be attributed to the transmission of radiation from the sample-driver plate interface, although as the

transmissivity does not exceed 5% at these wavelengths it would represent an extremely high interface temperature; however, this explanation is ruled out since the flash is seen in the HgCdTe band where the quartz is opaque. Another possibility is that it represents radiation from the shock front itself, although this seems improbable in view of the low times resolution of the detectors. Furthermore, if this were the case, the peak value would give a (low) estimate of the shock temperature, and the difference between it and the residual value could be used to estimate Grüneisen's parameter. The values obtained range from 27 to 2.17, while the thermodynamic Grüneisen's parameter for quartz is 0.7; this explanation would thus seem unacceptable. The most likely cause is triboluminescence, a phenomenon that has been documented in quartz by Nielson et al. (1961) who observed strong emission in the visible region of the spectrum from quartz shocked to similar pressures. In this case the black body temperature corresponding to the flash is unlikely to be significant.

Forsterite

Forsterite was the only material studied where the detector output for the two wavelength ranges was markedly different. For the range 4.5 to 5.75μ the records are similar to those obtained for quartz, and are characterised by a "flash" at about the time of the free surface arrival, followed by a level portion and subsequent rise to saturation. In fact, for the shots at 9.5 and 15.0 GPa two peaks, separated by ∿2 μs were observed, the first apparently preceding the free surface arrival; the first peak was lower amplitude and for pressures in excess of 15 GPa only one peak was observed. Records obtained using the HgCdTe detector showed no peak, but simply a rise to a level portion similar to that seen for metals and bronzite. Triboluminescence has not been documented in forsterite, and would not be expected to occur only in a limited wavelength range. The

most likely explanation for the change in signal is that the peaks represent transmitted radiation, since forsterite does have a transmission coefficient of up to 0.2 in the InSb range. If this is indeed the case, then the temperatures measured may tend to be slightly high as the driver plate and interface radiation will increase the signal.

The measured temperatures for forsterite are listed in Table 7 note that for pressures below the Hugoniot elastic limit (∿8.7 GPa; see Appendix B) there is no detectable rise in temperature and that the HgCdTe temperatures are lower, at least below 15 GPa. The latter observation is easily explained if there is some contribution to the InSb signal from transmitted radiation.

Bamble Bronzite ($(Mg_{0.86}Fe_{0.14})\ SiO_3$)

The records for Bamble bronzite were very similar for both wavelength ranges, and in fact resembled those obtained for metals in that there was no marked initial peak but simply a rise to a level portion used to determine the post-shock temperature, followed by a rise and eventual saturation. There was a slight peak observable in the InSb records; this is probably an artifact of the detector response, but could represent a lower limit on the shock temperature.

Temperatures determined for this material are listed in Table 8 the values are extremely similar for both wavelength ranges with the exception of the 25 GPa value. Between 20 and 25 GPa, the InSb temperature dropped by ∿25°C, whereas no corresponding drop was observed in the HgCdTe shots. The observed drop was probably due to the choice of sample: the Bamble bronzite is a natural single crystal which is permeated by fine cracks accounting for the 1% porosity reported by Gibbons (1974), and also contains some larger cracks. The presence of cracks can lead to high temperatures through localised heating, and the

sample shocked to 25.0 GPa was the least cracked, so might be expected to reach lower temperatures.

Comparison of Experimental and Theoretical Post-shock Temperatures

a. Commonly Used Calculational Techniques

The most widely used method of calculating shock, and hence post-shock, temperatures, is probably that developed for metals by Walsh and Christian (1955). If the entropy S is expressed as a function of temperature T and volume v, then the change in entropy is given by

$$dS = \left(\frac{\partial S}{\partial T}\right)_v dT + \left(\frac{\partial S}{\partial v}\right)_T dv \qquad (1)$$

Since $\left(\frac{\partial S}{\partial T}\right)_v = \frac{C_v}{T}$, where C_v is the specific heat at constant volume, and $\left(\frac{\partial S}{\partial v}\right)_T = \left(\frac{\partial P}{\partial T}\right)_v$ where P is pressure, this expression may be rewritten

$$TdS = C_v dT + \left(\frac{\partial P}{\partial T}\right)_v dv \qquad (2)$$

The energy conservation relation for the shock wave is

$$E_1 - E_0 = 1/2\ (P_1 + P_0)(v_0 - v_1) \qquad (3)$$

where E and P are energy and pressure, and the subscripts 1 and 0 refer to the shock and initial states. The first law of thermodynamics may be written

$$TdS = dE + P\ dv \qquad (4)$$

or, in integral form

$$\int_{S_1}^{S_0} [TdS]_{Hug} = E_1 - E_0 + \int_{v_0}^{v_1} [Pdv]_{Hug} \tag{5}$$

where the limits of integration refer to the initial and final shock states and the integration is performed along the Hugoniot. Substituting for $E_1 - E_0$ from (3) and differentiating with respect to v_1 yields the relation

$$\frac{d}{dv_1} \int_{S_0}^{S_1} [TdS]_{Hug} = \frac{dP}{dv_1} \frac{(v_0 - v_1)}{2} + \frac{P_1}{2} = f(v_1) \tag{6}$$

for a given Hugoniot. Combining this with (2) gives

$$\frac{d}{dv_1} \int_{S_0}^{S_1} [TdS]_{Hug} = C_v \frac{dt}{dV_1} \frac{1}{} + \left(\frac{\partial P}{\partial T}\right)_v T_1 = f(v_1) \tag{7}$$

which has the solution

$$T_1 (v_1) = To \exp \left(-\int_{v_0}^{v} b(v)dv \right) + \exp \left(-\int_{v_0}^{v} b(v)dv \right) \int_{v_0}^{v} \frac{f(v)}{C_v} \exp \left(\int_{v_0}^{v} b(v)dv \right) dv \tag{8}$$

where $b = \frac{1}{C_v} \left(\frac{\partial P}{\partial T}\right)_v = \frac{\gamma}{v}$ and γ = Grüneisen's parameter. A common simplifying assumption is that b is independent of volume, in which case (8) reduces to the form actually derived by Walsh and Christian, namely,

$$T_1(v_1) = To \exp\left(b(v_0 - v_1) + \exp(-bv_1) \int_{v_0}^{v} \left[\frac{f(v)}{C_v} \exp(bv)\right]_{Hug} dv \right. \quad (9)$$

Equations (8) and (9) may be reduced to difference equations and solved iteratively along the Hugoniot. C_v may either be assumed constant or specified at each point; the Debye formulation is often used, where

$$C_v = 3R\, C_D\left(\frac{\Theta_D(v)}{T}\right) \quad (10)$$

Here R is the gas constant, C_D is the Debye specific heat, normalised to 3R (see, e.g., American Institute of Physics Handbook (1972) Table 4e-8, page 4-113) and the volume dependence of the Debye temperature Θ_D is specified by

$$\Theta_D(v) = \Theta_D(v_0) \exp\left\{ - \int_{v_o}^{v} \frac{\gamma(v)}{v} dv \right\} \quad (11)$$

Temperatures T_s along an isentrope may also be derived from (7) which becomes

$$C_v \frac{dT_s}{dv_s} + \left(\frac{\partial P}{\partial T}\right)_v T_s = 0 \quad (12)$$

which has the solution

$$T_s = T_o \exp\left\{ \int_{v_0}^{v_s} \frac{\gamma(v)}{v} dv \right\} \quad (13)$$

where v_s is the volume on the isentrope.

In particular, the post-shock temperature T_R is given by

$$T_R = T_1 \exp \left\{ \int_{v_R}^{v_1} \frac{\gamma(v)}{v} \, dv \right\} \qquad (14)$$

where v_R is the release volume, often assumed to equal v_0.
In geophysical applications it is often assumed that the volume dependence of the Grüneisen parameter is given by

$$\gamma = \gamma_0 \left(\frac{v}{v_0} \right)^n \qquad (15)$$

($n \gtrsim 1$; the most commonly used value is in fact n = 1)
and γ is usually assumed to be independent of temperature.

Two assumptions have been made throughout this derivation: firstly that an ordinary fluid-type equation of state is valid, which ignores the effects of rigidity or elasto-plastic work, and secondly that thermodynamic equilibrium exists in states behind the shock front. In addition, because of the form used for the energy conservation, equation (3), the treatment is strictly valid only where the shock state is reached by a single step and not in the two-wave region associated with the Hugoniot elastic limit or phase changes; modifications are necessary in these cases.

An alternative approach was described in detail by Ahrens et al. (1969). The increase in internal energy ΔE_1 of a material shocked to a state with volume v_1 and pressure P_1 is given by equation (3) and is equated to the increase in internal energy resulting from isothermal compression at T_o from an initial volume to a final volume v_1 plus isovolumic heating to the shock temperature T_H. The energy increase along this path is given by

$$\Delta E_1 = \int_{v_0}^{v_1} \left(\frac{T\gamma C_v}{v} - P \right)_{T_o} dv + \int_{T_o}^{T_H} (C_v)_{v_1} dT \qquad (16)$$

where the temperature and volume dependence of the specific heat are described by the Debye Model. (The first term on the right hand side of (16) arises from the substitution of (2) into (4) with $dT = 0$.)

The pressure difference between the Hugoniot and the isotherm is given by

$$P_1 - P_T = b \int_{T_o}^{T_H} C_v \, dT \qquad (17)$$

where $b = \gamma/v$ is assumed constant. Hence the second term on the right hand side of (16) may be replaced by $\frac{P_1 - P_T}{b}$, giving

$$\Delta E_1 = \int_{v_0}^{v_1} \left(\frac{T\gamma C_v}{v} - P \right)_{T_o} dv + \frac{P_H - P_T}{b} \qquad (18)$$

Since ΔE_1 is given by (3), this equation may be solved for P_T, and T_H then determined from (17).

This formulation has the advantage that the effects of the Hugoniot elastic limit (P_e, v_e) and the two-wave structure resulting from it are readily included, for equation (3) may be written

$$\Delta E_1 = \frac{P_e(v_o - v_e)}{2} + \frac{(P_e + P_H)(v_e - v_H)}{2} \qquad (19)$$

It is also easily adapted for use in calculating shock temperatures in the high pressure regime for materials such as silicates which undergo phase changes. In this case the energy change ΔE_{PC} associated with the transition must be added to the change in internal energy associated with the isothermal compression followed by heating at constant volume

$$\Delta E_{HP} = \int_{v_o'}^{v_1'} (Tb'C_v' - P')_{T_o} \, dv + \int_{T_o}^{T_H} (C_v')_{v_1} dT + \Delta E_{PC} \qquad (20)$$

where the primed quantities refer to the high pressure phase, and the value of ΔE_{HP} given by (3) is substituted as before.

Calculations of temperatures in the mixed phase region are considerably more complicated, but the Hugoniot state is assumed to be a mixture of both high and low pressure phases in thermal and mechanical equilibrium. The internal energy in the shock state is given by the Rankine-Hugoniot conservation equation (3) and is equated to the sum of the energy changes produced by the isothermal compression of both phases to P_H, the isobaric heating of both phases from T_o to T_H, and a transformational energy term. Two equations are derived which may be solved numerically for the mass fraction of transformed material and the Hugoniot temperature at a series of points on the mixed phase Hugoniot.

In all cases, post-shock temperatures are calculated from the shock temperatures assuming adiabatic and usually isentropic expansion.

For cases where the release path is known, the residual temperature may be calculated directly, as described by Gibbons (1974). The energy in the Hugoniot state, given by (3), is equated to the change in internal energy due to the rise in temperature from the initial value T_o to the

residual value T_R plus the energy change along the release path. Thus

$$\Delta E = 1/2\ (P_1 + P_0)(v_0 - v_1) = \int_{v_1}^{v_R} [Pdv]_{release} + \int_{T_o}^{T_R} C_p\ dT \qquad (21)$$

where v_R is the volume on release.

The Hugoniot temperature may then be calculated from (15).

b) Results for Aluminium and Stainless Steel

Since the Walsh and Christian approach was developed specifically for application to metals (in the absence of phase changes) where the Hugoniot elastic limits are low ($\lesssim$0.2 GPa), the application of this technique should yield results in good agreement with the experimental observations. Figure 10 (a) and (b) show the values of shock (dashed lines) and post-shock temperature (solid curves) calculated for stainless steel-304 and aluminium-2024 using this approach; they are the same as those given by McQueen et al. (1970). Also plotted are the observed values, and, as can be seen, there is practically no agreement. In fact, the measured residual temperatures are, at low pressures, in excess of the calculated Hugoniot temperatures. Discrepancies between observed and theoretical residual temperatures in metals have also been reported by other workers (e.g., Von Holle and Trimble, 1976) using similar experimental techniques, and the question of the validity of the measurement arises. Certainly, the measured values may be too high because of surface processes or changes in emissivity -- though they are consistent in two wavelength ranges -- but the fact that they tend towards the theoretical values with increasing pressure suggests that the theory does not include some effect that dominates at low pressures. (Allowing for reasonable emissivity changes, the observed values are, in fact,

still higher than the calculated ones.) One obvious omission from the Walsh and Christian formalism is the effect of elasto-plastic work. Although the metals have low Hugoniot elastic limits, they retain some rigidity after yielding, and may undergo stress-hardening. The latter was reported by Fowles (1961), who demonstrated that an elasto-plastic equation of state should be used for aluminium shocked to pressures up to ∿15 GPa.

This concept was developed in detail by Lee and Liu (1967) and Lee and Wierzbicki (1967); briefly, the Rankine-Hugoniot law of conservation of energy is used in conjunction with a suitable material yield condition to derive a stress-temperature-strain relation characterising the response of the medium to a steady state shock wave. The calculations of the Hugoniot involve expanding the Helmholtz free energy per unit mass as a power series in elastic extensions and temperature, where the coefficients are related to the elastic constants, thermal expansion and specific heat of the material, and then using this to determine the stress, entropy and internal energy of the material. This treatment allows a direct calculation of temperature along the Hugoniot curve and incorporates the effects of material strength and finite anisotropic strain.

Foltz and Grace carried out the analysis for polycrystalline aluminium and copper; whilst their analysis may not be strictly valid for the aluminium alloy used in the present experiments, a comparison of their values for Hugoniot temperature (the dash-dot line in Figure 10(b)) and the measured residual temperatures is interesting. As can be seen, their calculated values are considerably in excess of the Walsh and Christian values at low pressures, but converge with them at higher pressures, which is precisely the behaviour observed in the measured residual

temperatures. Although the release path is not certain, it has been proposed that for metals the release from shock pressure P_H occurs in two stages: first an elastic release (isentropic) to a pressure $P_H - 2Y$, where Y is the Hugoniot elastic limit, followed by plastic release parallel to the Hugoniot (see e.g., Fowles, 1961; Al'tschuler, 1965). The post-shock temperatures indicated by the dotted curve in Figure 10(b) were derived from Foltz and Grace's Hugoniot temperatures assuming this form of release path with Y = 0.8 GPa. These values are in reasonable agreement with experimental observations (which may be slightly high due to changes in emissivity).

Unfortunately, the analysis carried out by Foltz and Grace is not strictly valid for an alloy like stainless steel, and the constants required for the calculation are not really defined in this case. However, the relationship between the observed and Walsh and Christian values (Figure 10(a)) is similar to that observed for aluminium, and plastic deformation of the lattice has been observed in recovery experiments for pressures up to 50 GPa (e.g., Murr, 1975; Smith, 1958). The post-shock temperatures indicated by the solid line in Figure 10(a) were calculated from the Hugoniot temperatures assuming a simple isentropic release path; some allowance for elasto-plastic behaviour may be made by assuming a release path as indicated above and calculating the residual temperatures directly using (21). This yields the dotted line in Figure 10-a, but the agreement between experiment and theory is not substantially improved.

It is concluded that elasto-plastic work, which is not included in the Walsh and Christian formalism, causes significant heating at low pressures resulting in large differences between measured and calculated temperatures. However, at higher pressures ($\lesssim$30 GPa for aluminium, $\lesssim$50 GPa for stainless steel) the Walsh and Christian approach appears to predict values close to those measured experimentally.

c. Application to Silicates

Comparison of Hugoniot curves for silicates and metals reveals several notable differences: the silicates have high Hugoniot elastic limits (generally $\gtrsim 5$ GPa) and undergo one or more phase changes which may begin at pressures as low as 14 GPa. In fact, because of the high Hugoniot elastic limit, the resulting two wave structure persists to high pressures and in those materials which begin to transform to high pressure phases at relatively low pressures (i.e., $\sim$14 GPa) the effects of dynamic yielding and the phase change may be hard to distinguish. Another difference between metals and some silicates is their behaviour on yielding: whereas metals retain some strength past the Hugoniot elastic limit, and elasto-plastic work is important, some silicates appear to undergo a rapid and complete loss of material strength, as was documented in detail for quartz by Wackerle (1962). Since the two-wave structure due to the yielding in silicates persists to high pressures where it may be replaced by a two-wave structure due to a phase change, the Walsh and Christian approach is not valid and must either be modified or replaced by some other calculational techniques such as that developed by Ahrens et al. (1969) and described earlier.

In his pioneering work on quartz, Wackerle (1962) circumvented the problem of the Hugoniot elastic limit by introducing an "equilibrium" Hugoniot obtained from a segmented linear fit to the plot of effective shock velocity U* against effective particle velocity u*, where U* and u* are given by

$$U^* = v_o(P/(v_o - v)]^{1/2} \tag{23}$$

$$u^* = [P(v_o - v)]^{1/2} \tag{24}$$

where v is the volume corresponding to a shock pressure P.

(These represent the true velocities only at high pressures where the two-wave structure no longer exists.) He then used this equilibrium Hugoniot and a modified form of the Walsh and Christian approach to calculate the shock and residual temperatures in quartz. His results are shown as the dashed and solid curves in Figure 11 (they have been corrected for an initial temperature of 24°C): the agreement between them and the observed post-shock temperatures is remarkably good except for the lowest and highest pressure points. (The latter may be in error due to the detector response anyway.) As was discussed earlier, most calculations assume the release volume is either the same as (as in this case) or greater than the initial volume, when it may in fact be less. A smaller release volume results in higher post-shock temperatures because less energy is lost on release. Lyzenga and Ahrens (1978) derived a relationship between the minimum post-shock volume v_o' and the free surface and particle velocities, U_{fs} and u_p, for a Hugoniot state (p_1, v_1), namely

$$v_o' \leq \frac{(U_{fs} - u_p)^2}{p_1} + v_1 \qquad (25)$$

This was used with Wackerle's data to estimate the release volumes for pressures of 5.6, 9.0, 11.6 and 18.4 GPa, and these values used to recalculate the post-shock temperatures which are plotted as asterisks in Figure 11 (a). Two additional points were calculated using measured release volumes from Grady et al. (1974). The agreement between these calculated values and the measurements is even better.

Mashimo et al. (1978) used release adiabat data to determine directly the residual temperatures in quartz in a manner analogous to that proposed

by Gibbons (1974). Their results are plotted as the heavy curve in Figure 11 (b): the agreement with the observations is excellent.

Figure 11 (b) also shows the results of applying the method of Ahrens et al. (1969) which includes the effect of the Hugoniot elastic limit in the temperature calculations. The values of 6 and 8 GPa used for the elastic limit are the upper and lower bounds on the "free run" limit for z-cut quartz given by Wackerle. These temperatures are much lower than the observed values, which are greater than the calculated shock temperatures even for the lower value of the Hugoniot elastic limit. (The discrepancy probably arises in the calculation of the isotherm.)

The dynamic compression of Bamble bronzite was studied by Ahrens and Gaffney (1971) and recovery experiments were carried out by Gibbons (1974). Bamble bronzite consists of large natural single crystals which are closely described by the formula $(Mg_{0.86}Fe_{0.14})SiO_3$; the theoretical zero-pressure density is 3.308 gm/cm^3 whereas the density of the samples used by Ahrens and Gaffney varied from 3.276 to 3.298 gm/cm^3 indicating a porosity of from 1 to 3%. This porosity is manifest in the fine cracks that permeate the samples, which also contain some larger cracks. The variation in porosity probably accounts for the considerable scatter in the Hugoniot data, and the decrease in temperature between 20 and 25 GPa observed in the InSb measurements. The material has a Hugoniot elastic limit of $\sim$6.7 GPa and undergoes a phase change to majorite (Smith and Mason, 1970) or possibly to ringwoodite plus stishovite (Ahrens and Gaffney, 1971), which begins at $\sim$14 GPa and is not complete until $\sim$40 GPa.

An attempt was made to determine an equilibrium Hugoniot, as defined by Wackerle (1962), using the data of Ahrens and Gaffney for the Bamble bronzite, but the (U*, u*) points were so scattered that no

obvious linear correlation existed, and the attempt was abandoned. Instead, theoretical Hugoniots were constructed from the Birch-Murnaghan adiabats using the constants of Table 9 and an initial specific volume of 0.304 cm^3/gm (for details of this method, see, e.g., Davies, 1974). Hugoniots were constructed for both values of γ (the differences arise from the different values of thermal expansion and specific heat used in calculating γ), and a value of $K'_{os} = 5.3$ was found to give a better fit to the observations, so was used throughout.

Figure 12 (a) indicates the results for the theoretical Hugoniot with $\gamma = 0.907$. The curves A and A' are the calculated shock and residual temperatures (using the Walsh and Christian method) and are considerably lower than the observations.

Calculations were also carried out, using the Walsh and Christian method, to investigate the effects of varying the behaviour of Grüneisen's parameter γ and the Debye temperature Θ_D (previously it was assumed that γ/v was constant and Θ_D independent of temperature, although the specific heats are fitted better if Θ_D is a function of temperature). The Hugoniot temperatures are relatively insensitive to Θ_D but are highly dependent on γ; however, if the same value of γ is then used to calculate the post-shock temperature, the latter varies very little. A model in which the Grüneisen parameter is higher on compression than release yields higher residual temperatures, however, it does not have a good physical basis, although the shock and release processes are certainly different. In particular, the observations of release paths lying beneath the Hugoniot (e.g., Figure 1) and the apparent hysteresis in the shock and release process are not fully understood; they may be related to the behavior of γ.

Curve B is the shock temperature for $\gamma = 2.5$ with the residual temperatures B' being calculated from B but assuming $\gamma = 1$ on release.

The agreement between B' and the observations is somewhat better, especially at high pressures, but a Grüneisen's parameter of at least 3 during shock compression would be required to produce agreement at pressures less than 15 GPa. In this case the calculated release temperatures (assuming $\gamma = 1$) would be too high at pressures of $\sim$25 GPa, so a more complicated behaviour of γ would have to be postulated. This does not seem justified since the theoretical Hugoniot does not adequately describe the effects of varying sample porosity, and the high temperatures may be largely due to this; furthermore, the effect of the phase change has been neglected -- although this would provide some justification for changing the behaviour of the effective γ at 15 GPa. The temperatures calculated using the approach of Ahrens et al. (1969) with a Hugoniot elastic limit of 6.7 GPa and a smooth fit to the observed Hugoniot points are plotted as curves C and C'; these are in even worse agreement with the observations.

Figure 12b illustrates the results of using $\gamma = 1.57$; the temperatures along the theoretical Hugoniot (D) are higher than those of curve A in Figure 12a, but the release temperatures given by D' are little different from A'. The calculations including the Hugoniot elastic limits also yield higher shock temperatures (E), but the residual temperatures are much lower.

Recovery experiments carried out by Gibbons (1974) on Bamble bronzite revealed considerably crushing and fracturing caused by the shock loading, and fine deformational twin lamellae. Above 17.3 GPa some undulatory extinction was apparent, and at 22.6 GPa a very small amount of glass was detected on the fractures. This suggests that the shock heating may be highly non-uniform, and the measured temperatures may thus be $\sim$ 20 to 30° higher than the mean material temperature.

In all these calculations the effects of the quartz to stishovite phase transition, which begins at ∿ 15 GPa and the phase change in bronzite (probably to majorite or ringwoodite plus stishovite) which starts at ∿ 13.5 GPa, have been ignored except in so far as the former changes the shape of the equilibrium Hugoniot. Examination of the experimental results suggests that there is a change in slope (of temperature versus pressure) at about 15 GPa in quartz corresponding to the change in Wackerle's calculated values; however, this is not marked, and there is no clear evidence of a change in the bronzite data associated with that transition. In quartz, the observations at pressures in excess of ∿ 20 GPa are less reliable owing to the triboluminescence; at this pressure the phase change is $\lesssim$ 25% complete (Grady et al. 1974) and it does not reach completion until ∿ 47 GPa. Although the properties of stishovite are fairly well known, calculation of reliable temperatures in the mixed phase regime is rather difficult; not only do the Hugoniot temperatures depend on how the phase change is modelled, but the release path, which strongly influences the residual temperature, is uncertain. Grady et al. suggest that it starts as unloading along a line of frozen concentration, but at ∿8 GPa the high pressure phase may transform to a low pressure (amorphous) phase. In view of these uncertainties, and the lack of reliable observations further into the mixed phase region, calculations of temperatures assuming a mixture of high and low pressure phases were not pursued; however, it may be noted that the high pressure phase in general reaches a much higher temperature: Mashimo et al. calculated residual temperatures in stishovite of 730° at 20 GPa and 1170°C at 30 GPa. Similar arguments apply to the bronzite, where the properties of the high pressure phase are less well defined, and the effect of variations in sample porosity is probably important.

The forsterite used in this study was a synthetic single crystal having a porosity of $\lesssim$1%. Unfortunately the Hugoniot for this particular material has not been determined at pressures below $\sim$50 GPa, but data are available for polycrystalline forsterite (McQueen, 1968) and for polycrystalline forsterite having an initial specific volume of 0.322 cm^3/g, or a porosity of $\sim$4% (Ahrens et al., 1971). These two sets of observations serve to define a reasonable Hugoniot, and indicate that the present measurements were all in the low pressure regime; however, the Hugoniot may not be entirely correct. The Hugoniot elastic limit for the material used was found to be 8.7 GPa (see Appendix B); this value is the result of a single experiment, and could perhaps be different for different samples. For this reason, calculations of Hugoniot and release temperatures using the technique of Ahrens et al. (1969) were made for assumed Hugoniot elastic limits of 5 and 9 GPa.

The available pressure volume data were used to derive equilibrium Hugoniots for the non-porous and porous samples in the manner used by Wackerle for quartz. The Walsh and Christian method was then used to calculate the Hugoniot temperatures; the final release volume was assumed, for both materials, to be the same as the initial volume of the non-porous sample, which will tend to yield a lower limit on the post-shock temperature. Temperatures were also calculated along a theoretical Hugoniot for single crystal forsterite, which was constructed from the Birch-Murnaghan adiabat using the constants given in Table 9 (for details of this method see e.g., Davies, 1974). The theoretical Hugoniot fitted the observed data quite well above 15 GPa.

The results of the temperature calculations are shown in Figure 13; at this stage it should be noted that the 10 and 15 GPa measurements using the InSb detector are probably contaminated by radiation from the sample

driver interface, as discussed previously. The observed temperatures are considerably in excess of the values calculated for the non-porous polycrystalline forsterite using the equilibrium Hugoniot (curves A, A', Figure 13 (a)), and are also greater than the values calculated for the theoretical Hugoniot (C, C') although there is some indication that the measurements tend towards the latter at high pressures. The values calculated for the "porous" equilibrium Hugoniot (B, B') are much higher than the observations except for the doubtful InSb points; this is not surprising since the samples were only ∿1% porous, and not 4%, but it does suggest that the measured temperatures might not be in great disagreement with theoretical values obtained from an appropriate equilibrium Hugoniot using actual release volumes.

Figure 13 (b) shows the calculated shock temperatures derived using the method of Ahrens et al. for Hugoniot elastic limits of 5 and 9 GPa (curves E and F) and residual temperatures (E') obtained from the 5 GPa curve. These values are significantly lower than the observations below ∿20 GPa, but the observed values tend towards them at higher pressures; as long as the measured value is lower than the calculated Hugoniot temperature, the discrepancy may be explained largely in terms of the release volume. However, the fact that the observations are initially higher than the shock temperatures, but converge with the calculations at high pressures is reminiscent of the behaviour observed in stainless steel and aluminium and ascribed to elasto-plastic effects. A detailed investigation of the process of dynamic yielding in forsterite would indicate whether such effects were possible here; if the behaviour of forsterite is indeed similar to that of metals, then the release path may be approximated by the two stage elastic-plastic path that was described earlier with reference to aluminium, and is sketched in Figure 14.

In this case an estimate of the release temperature may be obtained by calculating the energy difference between the shock and release paths (the shaded area in Figure 14) and equating it to the increase in internal energy as in equation 21. This results in the temperatures shown by the heavy line in Figure 13 (b); the agreement between these values and the observations is good at ∿10 GPa, but large differences exist at higher pressures, as would be expected if the material underwent a gradual loss of strength that was complete by ∿25 GPa. (Experimental evidence indicates that the loss of strength is in fact complete by ∿20 GPa; see Appendix B) This calculation ignored the fraction of energy going into permanent deformation of the lattice, which may be estimated as follows: the free energy of a crystal is increased by about $1/2\mu b^3$ per atomic length of dislocation, where μ is the shear modulus and b is the average length of the Burgers vectors of the crystals. With $b \sim 5\text{Å}$, μ = 80 GPa, and a dislocation density of 10^{11} cm^{-2}, which is probably rather high for these pressures (R. Jeanloz, personal communication, 1978), allowing for the deformational energy results in a 15% or smaller reduction in the increase in thermal energy due to shock compression and release. This is equivalent to a 6°C (or smaller) decrease in release temperatures from the values plotted in Figure 13 (b).

Attempts were also made to improve the agreement between observation and calculation by varying the behaviour of γ and Θ_D. As before, little change resulted, except when a higher value of Grüneisen's parameter was used on compression than on release. A fairly good fit to the data was obtained using the theoretical Hugoniot with γ = 2.5 on compression and 1 on release (curve D′ in Figure 13 (b)).

Discussion

The experimental technique described here has proved useful for measuring post-shock (brightness) temperatures in a variety of metals and silicates. Initial experiments have produced reproducible results which are, in general, consistent at two-wavelength ranges from 4.5 to 5.75μ and from 7 to 14μ. The reproducibility and consistency suggest that the measured temperatures are indeed representative of the residual temperatures in the shocked samples, although uncertainties still exist concerning the possible effects of changes in emissivity under shock conditions and of non-hydrodynamic surface processes.

Experiments on stainless steel and aluminium yielded measured values that were considerably in excess of those predicted by the Walsh and Christian model (1955) at low pressures, but tended towards the latter at higher pressures. This was attributed to elasto-plastic effects, which are well documented in aluminium and yield temperatures in reasonable agreement with the measurements. Other workers, such as Von Holle and Trimble (1976) have reported discrepancies between measured and residual temperatures that persist to much greater pressures (∿50 GPa) and apparently cannot be caused by elasto-plastic work; these have been ascribed to non-hydrodynamic surface heating. Surface effects are bound to affect measurements on metals where the infra-red optical depth is only $\sim 10^{-10}$m, and may be, in part, responsible for the differences between theory and observation reported in this study. However, the agreement between the temperatures predicted by the elasto-plastic theory and the observations for aluminium is quite good, and it is hard to see why the effect of surface heating should be dominant at low pressures and not at higher ones. One effect that may influence the measurements of residual temperatures in aluminium is the ejection of material from

the surface; this has been studied by Asay et al. (1976) for pressures of ∿25 GPa and is quite significant. A further study by Asay (1977) showed that material ejection was highly dependent on the rise-time of the shock wave, so the effect of material ejection on temperature measurement might be investigated by determining residual temperatures for different shock rise-times.

Comparison of observed and calculated temperatures for quartz indicate that the most reliable method for calculating residual temperatures is to do so directly using release adiabat data: agreement between the observations and the values of Mashimo et al. (1978) obtained in this manner was very good. There was also remarkably good agreement between values calculated using the 'equilibrium Hugoniot' technique of Wackerle (1962) and the observations, although since these were obtained from the Hugoniot temperatures assuming the release volume was equal to the initial volume, they may be further improved using actual or estimated release volumes which are smaller than the initial one.

Detailed release adiabat data were not available for forsterite or bronzite for the pressure range 5 to 30 GPa, and in fact, there is little good low pressure equation of state data available for forsterite; comparison of observed temperatures and those calculated in the optimal manner was thus not possible. The effect of the porosity and cracking in the Bamble bronzite probably leads to errors in the determination of theoretical temperatures. However, there is a considerable difference between the observed and calculated values, with the former being higher than the theoretical shock temperatures, although they do converge at higher pressures. For the forsterite also the measured temperatures were higher than those calculated on the Hugoniot, although there were some

indications that values obtained using the correct (but currently unavailable) equilibrium Hugoniot and estimated release volumes might not be so much lower than those measured . In both the forsterite and bronzite some process is required which results in higher shock temperatures at low pressures and less energy loss on release. An attempt was made to model such a process by allowing Grüneisen's parameter to be higher on compression than on release, and for forsterite reasonable agreement was obtained with $\gamma_o = 2.5$ on compression, $\gamma_o = 1$ on release (note that the thermodynamic Grüneisen's parameter is 1.17). No strict physical justification for postulating a different γ for shock compression from that on unloading is attempted here; however, this type of behaviour does provide better agreement between theory and observations although the model is somewhat non-unique. The differences between observed and predicted release adiabats and the hysteresis observed in shock unloading suggest that some change in material properties may occur prior to release from the shock state, and thus irreversible behaviour of the anharmonic properties is not incredible.

Although quartz has been observed to undergo a complete loss of material strength beyond the Hugoniot elastic limit (Wackerle, 1962), and elasto-plastic effects are probably not important in materials which undergo phase changes close to their elastic limits, there is no evidence to suggest that forsterite also completely loses strength for pressures greater than 9 GPa. Calculations of residual temperatures in which it was assumed that forsterite behaved in an elasto-plastic manner similar to that proposed for metals yielded values that agreed well with observations at 10 GPa but were much higher at higher pressures. This suggests that forsterite undergoes a much more gradual loss of material strength beyond its elastic limit than does quartz, and that elasto-plastic effects may be important at pressures below $\sim$25GPa.

The effects of surface heating on temperature measurement should be less severe in the silicates where the optical depth is microns. A more serious contriburion may result from non-uniform shock heating which has been clearly demonstrated in silicates where such features as adiabatic shear zones (e.g., Grady, 1977) deformational twin lamellae and localised production of glass (e.g., Gibbons, 1974) have been observed. This non-uniform heating is believed to contribute to the complete loss of strength once the Hugoniot elastic limit is exceeded. Quartz was the only material where a temperature rise was observed at pressures below the elastic limit, so perhaps non-uniform heating also occurs in the elastic regime. Both forsterite and enstatite showed a rapid rise in temperature once the Hugoniot elastic limit was exceeded. (An additional feature complicating the measurement of post-shock temperatures in quartz is the initial "flash" which has been associated with triboluminescence.)

The good agreement between theory and observations for quartz yet apparent large discrepancies for forsterite and bronzite raises the question of inherent differences between these materials. Their behaviour on compression is certainly very different: quartz is much more compressible (and is also less dense initially). There is a possibility that framework silicates (such as quartz) and chain silicates (such as bronzite) or neso-silicates (like forsterite) react differently under stress. The feldspars, which are also framework silicates, have similar initial densities to quartz and are also quite compressible (Ahrens et al., 1969); since release adiabat data are available for feldspars such as oligoclase, they are logical materials to investigate with the technique developed in this study in order to clarify this point, and also to substantiate the claim that the optimal method for calculating residual temperatures is directly from release adiabat data.

It has been emphasised throughout that the release path is of critical importance to the determination of post-shock temperatures, yet it has generally been assumed that the release is isentropic; if this is not the case, then discrepancies between measurement and theory are not surprising. Waldbaum (1971) suggested that release from shock might be isenthalpic rather than isentropic, and thus cause heating rather than cooling for many materials including silicates. Heating on release instead of cooling would certainly solve the problem of measured post-shock temperatures being higher than theoretical Hugoniot temperatures, but this hypothesis would not explain the convergence of measured and calculated values at high pressures. However, the assumption that the adiabatic release is in fact isentropic may not be strictly valid, although unless the real release path is known it is hard to correct for this effect. A more detailed analysis of the requirements for isentropic release by Kieffer and Delany (1978) suggests that it will only occur for low viscosity ($< \sim 10^6$ poises) materials, and that the assumption of isentropic flow in solids under decompression may thus be invalid because viscous dissipation is significant. Viscous heating on release would account for residual temperatures that are higher than those calculated on the Hugoniot, and would also presumably be more important at low pressures where lower Hugoniot temperatures imply a higher viscosity.

Release adiabats which lie below the Hugoniot (see Figure 1) lead to higher residual temperatures in better agreement with the observations, yet it seems strange that, if the material is essentially unchanged by shock compression and release, it should occupy a smaller volume on release when it is hotter than it was initially. Measurements of the

parameters on release adiabats are often made at relatively high pressures ($P_H > P_R >> 0$, where P_H is the shock pressure and P_R the point at which release measurements are made) and so yield information on the initial slope of the release adiabat which may then be extrapolated to yield the release volume. Such an extrapolation is illustrated schematically in Figure 15 by the dashed line: this yields a release volume smaller than v_0; however the actual path may be as shown by the dotted line. Since the area between the Hugoniot and the two release curves is the same, they will give the same residual temperatures if (21) is used. Assuming that the material is unchanged, then the release volume may be estimated from the post-shock temperature and the thermal expansion coefficient α_v, and can provide additional constraints on the release path. Table 10 lists the estimated release volumes for the materials studied: in fact, for the silicates and stainless steel they are not very different from the initial volumes.

Classifications of shock-metamorphism such as that of Stoffler (1971) are generally based on calculated values of shock and residual temperatures, and should be re-evaluated in the light of the present study. Stoffler based his classification on the calculations of Wackerle (1962) for quartz and Ahrens et al. (1969) for feldspars. The measurements of this study indicate that Wackerle's results are probably fairly reliable below ~20 GPa, although it is important that they be corrected for the right initial temperatures and, where possible, for the actual release volume. They may also be rather low for pressures well into or above the mixed phase region. (The work of Mashimo et al. (1978), which is in good agreement with the present study, indicates that Wackerle's values for both shock and residual temperature are low up to ~70GPa.) No measurements have been made for

feldspars, but it may be noted that the calculational technique of Ahrens et al. (1969) yielded rather too low post-shock temperatures for all the materials studied here, and hence the values used by Stoffler may also be too low. The main implication of this study for impact metamorphism is that temperatures in forsterite and bronzite appear considerably higher than the theoretical values, especially for porous samples, and so the effects of impact metamorphism on basic rocks such as lunar basalt may differ from those expected on the basis of theory and lead to erroneous conclusions regarding the nature of the impact. Since the partition of energy during impact processes is important in calculating the thermal history of an accreting planet, residual temperature data such as those presented here could provide useful constraints on the temperature distribution during accretion.

It was hoped that this study would yield some definite information on the behaviour of Grüneisen's parameter, which is critical for the reduction of shock wave data to the form needed for comparison with density-depth profiles within the earth. However, post shock temperatures are not very sensitive to the behaviour of γ (unless it is different on shock compression and release) and appear more greatly influenced by the release path, in particular the release volume. There seems to be no need to postulate unusual behaviour of γ for quartz to $\sim$25 GPa, although the high observed values of residual temperatures in forsterite and bronzite suggest that present rheological models used in shock temperature calculations, at least below $\sim$25 GPa, are either inadequate, or the effective Grüneisen parameter is high ($\gamma_o \sim 2.5$) on compression and decreases to near its zero pressure value ($\gamma_o \sim 1$) upon adiabatic release.

Acknowledgements

The authors thank Raymond Jeanloz and Gregory Lyzenga for many interesting and stimulating discussions; they are also indebted to Wayne Miller and Vic Nenow, who designed and built the variable gain amplifier used with the InSb detector, and to the staff of the Santa Barbara Research Centre, Goleta, California for their advice concerning detector operation. This work was supported by NASA under grant NGL 05-002-105. Contribution No. 3143, Division of Geological and Planetary Sciences, California Institute of Technology, Pasadena, California 91125.

Table 1

CALCULATED POST SHOCK TEMPERATURES
IN FUSED QUARTZ AND OLIGOCLASE,

using the Mie-Grüneisen Theory (A) or Release Adiabat Data (B)

Shock Pressure GPa	Post Shock Temperatures, °C			
	Fused Quartz		Oligoclase	
	A[1]	B[2]	A[3]	B[4]
10.0	0	80		
15.0	0	450		
18.0			27 - 35	269-386
25.0	0	1220		
27.2			129-206	> 742
30.0	470	1480		
40.0	1860	2180		
41.7			327-395	>1031
50.0	3310	2820		

1. Wackerle (1962)
2. Gibbons and Ahrens (1971)
3. Ahrens et al. (1969)
4. Ahrens and O'Keefe (1972)

Table 2

POWER LAW FITS TO CALIBRATION CURVES

$S = a(T-24)^b \times 10^{-5}$; coefficient of determination r^2

	Black Body			Stainless Steel			Aluminium-2024		
	a	b	r^2	a	b	r^2	a	b	r^2
InSb	7.21	1.87	.99	2.21	1.93	.98	3.08	1.71	.95
HgCdTe	10.9	1.45	.97	10.05	1.32	.97	2.68	1.43	.98

Table 3

MEASURED POST-SHOCK TEMPERATURES

IN STAINLESS STEEL-304

Temperature, °C

	InSb		HgCdTe		Peak
Pressure, GPa	SS	BB	SS	BB	(InSb)
11.5			80	60	
11.7	110	75			250
13.0	125	80			600
14.5			130	85	
16.0	145	100	145	95	830
23.0	195	130			1530
24.2			200	130	
43.0	325	230			
50.0	355	250			1820

SS = calibration using stainless steel

BB = black body temperature

Uncertainties in temperature: ±15° below 150°, ±10° above 150°.

T_o = 24°C

Table 4

MEASURED POST-SHOCK TEMPERATURES

IN ALUMINIUM-2024

Temperature, °C

Pressure, GPa	InSb		HgCdTe		Peak (InSb)
	AL	BB	AL	BB	
10.5	125	50			
11.5			140	65	
12.5	135	55			1250
15.0	150	60			
15.7			155	70	
18.5	175	75	185	80	1430
25.0			220	90	
27.0	230	105			2200
32.5	250	120			
33.0	260	127			3800

AL = calibration with aluminium

BB = equivalent black body temperature

Estimated uncertainties: ±20°C below 200°C, ±10°C above 200°C

T_o = 24°C

Table 5

ESTIMATED SIGNAL CORRECTION FACTORS

$$\text{Correction factor} = \frac{S \text{ silicate}}{S \text{ Black body}} \quad \text{(values to nearest .05)}$$

	T = 400°K	T = 600°K
InSb		
Quartz (polished)	.90	.85
SiO_2 (crystalline)	.90	.90
Dunite (polished)	.85	.80
(Bronzite	.9	.9)
HgCdTe		
Quartz (polished)	.80	.80
Quartz (rough)	.90	.90
Dunite (polished)	.90	.90
(Bronzite	.85	.85)

Table 6

MEASURED POST-SHOCK TEMPERATURES IN QUARTZ

Temperature, °C

	InSb			HgCdTe		
Pressure, GPa	Flash	BB	Corr.	Flash	BB	Corr.
5.0	235	80	87			
5.5				110	75	85
8.0	180	100	105			
9.5	225	120	125	320	115	127
10.8	245	155	162			
11.5	252	160	170			
15.0	340	177	187			
15.5*				--	160	180
17.5	377	185	195			
19.5				706	320	340
20.0	390	242	255			
21.5	425	250	265			

*This was a very faint record, and may not be reliable.

Uncertainties: ±10°C below 100°C, ±5°C above 100°C

T_o = 24°C

Table 7

MEASURED POST-SHOCK TEMPERATURES IN FORSTERITE

Temperature, °C

	InSb			HgCdTe	
Pressure, GPa	Flash	BB	Corr.	BB	Corr.
7.5	180	<50°	(no detectable rise)		
9.6*	237	105	115	65	77
15.0**	260	136	145		
18.0				105	112
20.2	285	140	152		
21.0				120	125
24.0				160	165
24.5	270	148	160		
28.0	300	156	167		

*Two peaks (175, 237°C); residual temperature corresponds to the difference between the levels after the second and first peaks.

**Two peaks (135, 260°C); residual temperature estimated as before.

Estimated uncertainties: ±10°C below 100°C, ±5°C above 100°C

T_o = 24°C

Table 8

MEASURED POST-SHOCK TEMPERATURES IN BAMBLE BRONZITE

Pressure, GPa	Temperature, °C				
	Peak	BB	Corr.	BB	Corr.
6.0		$\lesssim$ 50° (no detectable rise)			
10.3	123	100	105		
11.0				110	120
14.8				145	160
15.5	185	147	157		
20.7	225	200	213		
21.5				185	200
25.0	200	175	185		
26.0				225	240

Uncertainties: ±10°C below 100°C, ±5°C above 100°C

T_o = 24°C

Table 9

SOME CONSTANTS RELEVANT TO THE CALCULATION

OF TEMPERATURES IN SHOCKED SILICATES

	ρ_o^{-1} cm^3/gm	γ_o	Θ_D[1] °K	$\bar{m}$	K_{os} GPa	K'_{os}
Quartz	.377	.703[2]	1050	20.03	37.7[2]	6.4[2]
Forsterite	.310	1.17[2,3]	900	20.12	126.7[3] 128.8[4]	5.37[3]
Bronzite	.298[5]	.907	950	20.96	103.5[5]	9.59[5]
	.307	1.56[5]			105.0[7]	5.3[6]

γ_o = thermodynamic Grüneisen parameter

Θ_D = Debye temperature

$\bar{m}$ = mean atomic weight

K_{os} = zero pressure adiabatic bulk modulus

$$K'_{os} = \left(\frac{\partial K_{os}}{\partial P}\right)_T$$

1. Debye temperatures derived from fitting specific heat data from J.A.N.A.F. Tables.
2. Values from Anderson et al. (1968)
3. Kumazawa and Anderson (1969)
4. Graham and Barsch (1969)
5. Frisillo and Barsch (1971) $[Mg_{0.8}Fe_{0.2})SiO_3]$
6. Chung (1971)
7. Kumazawa (1969)

Note: $\frac{\gamma}{v}$ was generally assumed constant.

Table 10

ESTIMATED RELEASE VOLUMES

	Al-2024	SS-304	Quartz	Forsterite	Bronzite
v_o (cm^3/g)	0.359	0.127	0.377	0.310	0.302+
$\bar{\alpha}_v$ (K^{-1})	8×10^{-5}	5×10^{-5}	3.5×10^{-5}	2.6×10^{-5}	2.4×10^{-5}
Pressure, GPa					
5	--	--	0.3776	∿0.310++	∿0.302++
10	0.361	0.1274	0.3782	0.3104	0.3026
15	0.363	0.1276	0.3789	0.3105	0.3029
20	0.364	0.1279	0.3799	0.3107	0.3032
25	0.365	0.1281	--	0.3111	0.3031/ 0.3035

+ Theoretical zero-pressure density, (Ahrens & Gaffney, 1971)
Actual initial volume ∿0.304 cm^3/g

++ No detectable temperature change

References:

Ahrens, T. J., D. L. Anderson and A. E. Ringwood, Equations of state and crystal structures of high-pressure phases of shocked silicates and oxides, Rev. Geophys., 7, 667-707, 1969.

Ahrens, T. J. and E. S. Gaffney, Dynamic compression of enstatite, J. Geophys. Res., 76, 5504-5513, 1971

Ahrens, T. J., W. H. Gust and E. B. Royce, Material strength effect on the shock compression of alumina, J. Appl. Phys., 39, 4610-4616, 1968.

Ahrens, T. J., J. H. Lower and P. L. Lagus, Equation of state of forsterite, J. Geophys. Res., 76, 518-528, 1971.

Ahrens, T. J. and J. D. O'Keefe, Shock melting and vaporization of lunar rocks and minerals, The Moon, 4, 214-249, 1972.

Ahrens, T. J., J. D. O'Keefe and R. V. Gibbons, Shock compression of a recrystallized anorthositic rock from Apollo 15, Proc. Lunar Sci. Conf. 4th, 2575-2590, 1973.

Ahrens, T. J. and C. F. Petersen, Shock wave data and the study of the earth in The Application of Modern Physics to the Earth and Planetary Interiors, S. K. Runcorn, ed., 449-461, Wiley-Interscience, 1969.

Ahrens, T. J., C. F. Petersen and J. T. Rosenberg, Shock compression of feldspars, J. Geophys. Res., 74, 2727-2746, 1969.

Al'tschuler, L. V., Use of shock waves in high pressure physics, Sov. Phys. Usp., 8, 52-91, 1965 (English Trans.).

American Institute of Physics Handbook, D. E. Gray, ed., McGraw-Hill, 3rd Edition 1972, Table 4e-8, page 4-113.

Anderson, O. L., E. Schreiber, R. C. Liebermann and N. Soga, Some elastic constant data on minerals relevant to geophysics, Rev. Geophys., 6, 491-524, 1968.

Asay, J. R. Effect of shock-wave rise time on material ejection from aluminium surfaces, Sandia Laboratories Report SAND77-0731, 1977.

Asay, J. R., L. P. Mix and F. C. Perry, Ejection of material from shocked surfaces, App. Phys. Lett., 29, 284-287, 1976.

Buettner, K. J. K. and C. D. Kern, The determination of infrared emissivities of terrestrial surfaces, J. Geophys. Res., 70, 1329-1337, 1965.

Burns, R. G., Mineralogical Applications of Crystal Field Theory, Ch. 4, pp. 49-77, Cambridge University Press, 1970.

Chung, D. H., Equations of state of pyroxenes in the (Mg, Fe)SiO_3 system, EOS Trans. Am. Geophys. U., 52, 919, 1971 (abstract).

Davies, G. F., Limits on the constitution of the lower mantle, Geophys. J. R. astr. Soc., 38, 479-503, 1974.

Duvall, G. E. and G. R. Fowles, Shock waves, Chapter 9, in High Pressure Physics and Chemistry, Volume II, R. S. Bradley, ed., Academic Press, London, 209-291, 1963.

Foltz, J. F. and F. I. Grace, Theoretical Hugoniot stress-temperature-strain states for aluminum and copper, J. Appl. Phys., 40, 4195-4199, 1969.

Fowles, G. R., Shock wave compression of hardened and annealed 2024 aluminum, J. Appl. Phys., 32, 1475-1487, 1961.

Fowles, G. R., Dynamic Compression of quartz, J. Geophys. Res., 72, 5729-5742, 1967.

Frisillo, A. L. and G. R. Barsch, Measurement of single-crystal elastic constants of bronzite as a function of pressure and temperature, J. Geophys. Res., 77, 6360-6384, 1972.

Gibbons, R. V., Experimental effects of high shock pressure on materials of geological and geophysical interest, Ph.D. Thesis, California Institute of Technology, 1974.

Gibbons, R. V. and T. J. Ahrens, Shock metamorphism of silicate glasses, J. Geophys. Res., 76, 5489-5498, 1971.

Goto, T., G. R. Rossman and T. J. Ahrens, Absorption spectroscopy in solids under shock compression, Proc. 6th AIRAPT International High Pressure Conference, Boulder, Colorado, 1977 (in press).

Grady, D. E., Processes occurring in shock wave compression of rocks and minerals, in High Pressure Research: Applications in Geophysics, M. H. Manghnani and Syun-Ibi Akimoto, eds., Academic Press, New York, 359-435, 1977.

Grady, D. E., W. J. Murri and G. R. Fowles, Quartz to stishovite: wave propagation in the mixed phase region, J. Geophys. Res., 79, 332-228, 1974.

Graham, E. K., Jr. and G. R. Barsch, Elastic constants of single-crystal forsterite as a function of temperature and pressure, J. Geophys. Res., 74, 5949-5960, 1967.

J.A.N.A.F. Thermochemical Tables, Nat. Stand. Ref. Data Ser., Nat. Bur. Stand. (U.S.), 37, 1141 pp., 1971.

Kieffer, S. W. and J. M. Delany, Isentropic decompression of fluids from crustal and mantle pressures, Manuscript submitted for publication, 1978.

King, D. A., and T. J. Ahrens, Shock compression of ilmenite, J. Geophys. Res., 81, 931-935, 1976.

King, P. J., D. F. Cotgrove and P. M. B. Slate, Infra-red method of estimating the residual temperature of shocked metal plates, in Behaviour of Dense Media under High Dynamic Pressures, J. Berger, ed., Gordon and Breech, 513-520, 1968.

Kormer, S. B., Optical study of the characteristics of shock-compressed condensed dielectrics, Sov. Phys. Usp., 11, 229-254, 1968.

Kormer, S. B., M. V. Sinitsyn, G. A. Kirillov and V. D. Urlin, Experimental determination of temperature in shock-compressed NaCl and KCl and of their melting curves at pressures up to 700 Kb, Sov. Phys. J.E.T.P. 21, 659-700, 1965.

Kumazawa, M., The elastic constants of single-crystal orthopyroxene, J. Geophys. Res., 74, 5973-5980, 1969.

Kumazawa, M. and O. L. Anderson, Elastic moduli, pressure derivatives and temperature derivatives of single-crystal olivine and single-crystal forsterite, J. Geophys. Res., 74, 5961-5972, 1969.

Lee, E. H. and D. T. Liu, Finite-strain elastic-plastic theory with application to plane-wave analysis, J. Appl. Phys., 38, 19-27, 1967.

Lee, E. H. and T. Wierzbicki, Analysis of the propagation of plane elastic-plastic waves at finite strain, J. Appl. Mech., 34, 931-936, 1967.

Lyon, R. J. P., Analysis of rocks by spectral infrared emission (8 to 25 microns), Econ. Geol., 60, 715-736, 1965.

Lyzenga, G. A. and T. J. Ahrens, The relation between the shock-induced free surface velocity and the post-shock specific volume of solids, J. Appl. Phys., 49, 201-204, 1978.

Mashimo, T., K. Nishii, T. Soma, A. Sawaoka and S. Saito, Some physical properties of amorphous SiO_2 synthesized by shock compression of α-quartz, Submitted for publication, 1978.

McQueen, R. G., Shock wave data and equations of state, in Seismic Coupling, G. Simmons, ed., Advanced Research Projects Agency Meeting, 1968.

McQueen, R. G. and S. P. Marsh, Equations of state for nineteen metallic elements from shock-wave measurements to two megabars, J. Appl. Phys., 31, 1253-1269, 1960.

McQueen, R. G., S. P. Marsh, J. W. Taylor, J. N. Fritz and W. J. Carter, The equation of state of solids from shock wave studies, Chapter VII, in High-Velocity Impact Phenomena, R. Kinslow, ed., Academic Press, 293-417, 1970 (see also Appendix C, D, E, pp. 518-520, 521-529, 530-568).

Murr, Lawrence E., Interfacial Phenomena in Metals and Alloys, Addison Wesley, pp. 326, 348, 349, 1975.

Nielson, F. W., W. B. Benedick, W. P. Brooks, R. A. Graham and G. W. Anderson, Electrical and optical effects of shock waves in crystalline quartz, in Colloques Internationaux du Centre National de la Recherche Scientifique, No. 109, Les Ondes de Détonation, 391-414, 1961.

Raikes, S. A., Post-shock temperatures: their experimental determination, calculation and implications, Ph.D. Thesis Part II, California Institute of Technology, 1978.

Schneider, E. and A. Stilp, Measurement of temperature distributions within steel targets impacted by hypervelocity projectiles: method and preliminary results, Paper presented at the 7th International Congress on Instrumentation in Aerospace Simulation Facilities, RMCS, Shrivenham, England, September, 1977.

Smith, C. S., Metallographic studies of metals after explosive shock, Trans. Metall. Soc. of AIME, 212, 574-589, 1958.

Smith, J. V. and B. Mason, Pyroxene-garnet transformation in coorara meteorite, Science, 168, 832-833, 1970.

Stoffler, D., Progressive metamorphism and classification of shocked and brecciated crystalline rocks at impact craters, J. Geophys. Res., 76, 5541-5551, 1971.

Stoffler, D., Deformation and transformation of rock-forming minerals by natural and experimental shock processes. 1. Behaviour of minerals under shock compression, Fortschr. Miner. 49, 50-113, 1972.

Taylor, J. W., Residual temperatures in shocked copper, J. Appl. Phys., 34, 2727-2731, 1963.

Touloukian, Y. S. and D. P. DeWitt, Thermal radiative properties, non-metallic solids, T.P.R.C. Data Series, 8, Plenum Press, 1972.

Urtiew, P. A. and R. Grover, Radiation temperature in solids under shock loading, Fifth Symposium on Temperature, its Measurement and Control in Science and Industry, Nat. Bur. Stand., 4, 677-684, 1973 (Am. Inst. Phys.).

Urtiew, P. A., Effect of shock loading on transparency of sapphire crystals, J. Appl. Phys., 45, 3490-3493, 1974.

Urtiew, P. A. and R. Grover, Temperature deposition caused by shock interactions with material interfaces, J. Appl. Phys., 45, 140-145, 1974.

Von Holle, W. G. and J. J. Trimble, Temperature measurement of shocked copper plates and shaped charge jets by two-colour IR radiometry, J. Appl. Phys., 47, 2391-2394, 1976.

Wackerle, J., Shock compression of quartz, J. Appl. Phys., 33, 922-937, 1962.

Waldbaum, D. R., Temperature changes associated with adiabatic decompression in geological processes, Nature, 232, 545-547, 1971.

Walsh, J. M. and R. H. Christian, Equation of state of metals from shock wave measurements, Phys. Rev., 97, 1544-1556, 1955.

Appendix A Detector parameters.

Both detectors were purchased from the Santa Barbara Research Centre, Goleta, California.

a) InSb

The InSb detector used was a circular chip 1 mm in diameter having a detectivity of 5×10^{10} cm $Hz^{1/2}$/watt when operated at 77°K. It was operated with a fast matched pre-amplifier (S.B.R.C. Model A-230) consisting of a current mode operational amplifier with a feedback resistance of 1 kΩ and a non-inverting voltage mode post-amplifier; this stage had a gain of 500, and upper and lower 3db frequencies of 20 MHz and 1.35 kHz respectively. For use in measuring post-shock temperatures an additional amplifier with variable gain (from 1000 to 30,000) was used (Raikes, 1978). The minimum system rise time of ∿0.1μs is controlled by the detector chip itself. Sapphire windows were used with this detector.

b) HgCdTe

The chip used had an area of 2×10^{-2} cm^2, a detectivity of 6.94×10^9 cm $Hz^{1/2}$/watt and a rise time of ∿ 100 nsec. It was used with a matched amplifier, S.B.R.C. Model A-120, having a gain of 1000. The amplifier consisted of an a-c coupled voltage mode amplifier plus a 499 Ω load resistor and circuitry to produce the bias current of 10 mA required by the detector; its upper and lower 3db frequencies were 10 MHz and 50 Hz respectively. The rise time of the detector-amplifier system is ∿ 0.05 μs; however, for operation at low signal levels it was found to produce an unacceptable level of very high frequency noise, and so had to be operated with a filter which raised the rise-time to ∿ 0.75μs. Barium fluoride or Irtran-2 (Kodak) windows were used with the HgCdTe detector.

Appendix B Dynamic Yielding in Forsterite

A detailed study of the dynamic yielding of single crystal forsterite has not been carried out. For the purpose of the present work a single measurement of the Hugoniot elastic limit along the c-axis of forsterite was undertaken in order to place some bounds on the rheological behaviour at relatively low shock stress.

Shock loading and recording were carried out with a modification of the 40 mm gun system described in Ahrens et al., 1971, 1973, although the optical recording was carried out using a Model 339B Beckman and Whitley continuous writing streak camera with a recently constructed xenon light source (described in Goto et al., 1978).

The sample, machined from the same aliquot as that utilised for the post-shock temperature measurements, was mounted on a 1.5 mm thick aluminium-2024 driver plate and impacted with a 4mm thick aluminium-2024 flyer plate. The pertinent measurements obtained in a single experiment (Figure B-1, Table B-1) provide a rather unequivocal measurement of the Hugoniot elastic limit amplitude, 8.68 ± 0.67 GPa, for a 3.7 mm thick sample. The velocity of the first shock, 8.72 km/s, is close to, but slightly higher than, the values of 8.543 km/s (Kumazawa and Anderson, 1969) or 8.564 km/s (Graham and Barsch, 1969) measured for the longitudinal velocity in the (3) direction. A similar relationship between the two velocities has been reported for quartz in various orientations (Wackerle, 1962; Fowles, 1967). The theoretical relation of the higher order elastic constants to the velocity of finite strength elastic waves, although reported for hexagonal symmetry (Fowles, 1967) has not been worked out for orthorhombic crystals.

The arrival time of the second shock, as indicated by the marked change in slope observed in the image of the inclined mirror (Figure B-1), can be interpreted in several ways depending on the rheology assumed for the sample material which has been compressed, and subsequently released, by the first shock (Wackerle, 1962). Our preferred analysis is simply to assume that the second shock velocity is given by

$$\overline{U}_2 = \frac{d + U_{1fs}\,(t_2-t_1)}{t_2-t_0} \qquad \text{B-1}$$

where d is the sample thickness, U_{1fs} the free surface velocity and (t_2-t_1) and (t_2-t_0) are the time interval between the arrival of the first and final shock and the travel time of the second shock to the free surface respectively (Ahrens et al., 1968). Equation B-1 ignores the interaction of the reflection of the first shock with the oncoming final shock front. The parameters of the final shock state (Table B-1) were obtained from an impedance match solution using the equation of state parameters given by McQueen et al. (1970) for aluminium-2024. Equation B-1 yields a final shock state which agrees well with the pressure-density trajectory calculated via the Murnaghen equation using parameters obtained from the ultrasonic data. If, on the other hand, the expression for the final shock velocity given by Ahrens et al. (1973), which assumes an elastic interaction of the reflected elastic shock with the oncoming final shock, is used a state with a greater compression is calculated (Figure B-2). Although the difference between the two solutions is not large, the calculation assuming no interaction, implying a loss of strength at pressures corresponding to the final shock state, appears to be definitely more consistent with the ultrasonic data. The relatively high Hugoniot elastic limit, followed by a (gradual) loss of shear strength, is consistent with the rheological behaviour inferred from the post-shock temperature measurements (Table 7).

Table B-1

Equation of State Data for Forsterite Shocked

Along the (001) Direction

(Shot 431)

Sample Mass	3.1546 ±0.0001g
Bulk Density	3.2158 ±0.005 gm/cm^3
Projectile Velocity	1.668 ±0.002 km/s

	First Shock State	Final Shock State
Shock velocity	8.717 ±0.068 km/s	6.554 ±0.067 km/s
Shock density	3.334 ±0.008 gm/cm^3	3.5716 ±0.0041 gm/cm^3
Shock pressure	8.68 ±0.67 GPa (Hugoniot elastic limit)	17.32 ±0.05 GPa
Free surface velocity	0.619 ±0.042 km/s	
Particle velocity		0.7246 ±0.0022 km/s

Figure Captions

Figure 1. Schematic diagram of Hugoniot and possible release adiabats. The solid release curves lie above the Hugoniot, and the dashed ones below it.

Figure 2. Schematic diagram of the experimental configuration. An oscilloscope recording the detector output at 50 μs/div is triggered by the passage of the projectile past the first laser beam. A record having greater time resolution (5 μs/div) is obtained from an oscilloscipe triggered by the impact of the projectile with the shorting target.

Figure 3. (a) Response curve for InSb detector material.
(b) Response curve for HgCdTe detector material.
Shaded areas indicate typical variations in detector sensitivity.
(Details from the Santa Barbara Research Centre Catalogue)

Figure 4. Infra-red transmission scans for the silicate materials studied. The operating range of the filtered InSb detector and the start of the HgCdTe band are also shown.

Figure 5. Calibration curves for the InSb detector, operating in the wavelength range 4.5 to 5.75μ. The open and solid circles in the aluminium curve are the results of two different calibration runs.

Figure 6. Calibration curves for the HgCdTe detector.

Figure 7. InSb detector output records for aluminium and stainless steel. T_1 = residual temperature, T_2 = peak temperature, A = air shock.

Figure 8. InSb detector output records for the silicates studied. T_1 = flash temperature, T_2 (or T) = residual temperature.

Figure 9. HgCdTe detector output records for the silicates studied. T = residual temperature.

Figure 10. Comparison of observed and calculated temperatures in (a) stainless steel and (b) aluminium. The dashed curves are the Hugoniot temperatures calculated using the Walsh and Christian technique, and the solid curves the corresponding release temperatures. The dotted curve in (a) represents residual temperatures calculated directly assuming elasto-plastic release. The dot-dash and dotted curves in (b) are the shock and post-shock temperatures obtained using the treatment of Foltz and Grace (1969).

Figure 11. Comparison of observed and calculated temperatures in quartz. In (a) the dashed line and solid line are the values of Wackerle (1962), corrected for T_o = 24°C. In (b) the dashed lines are Hugoniot temperatures calculated using the method of Ahrens *et al.* (1969) for the indicated values of Hugoniot elastic limit; the solid curve labelled 6 GPa are the corresponding release temperatures. The heavy solid line shows the values of Mashimo *et al.* (1978).

Figure 12. Observed and calculated temperatures for Bamble bronzite. Solid curves are post-shock temperatures, broken curves Hugoniot temperatures.

(a) A, A^1 : theoretical Hugoniot γ = .907

B, B^1 : theoretical Hugoniot, γ = 2.5 on compression, 1 on release

C, C^1 : actual Hugoniot, γ = .907, Hugoniot elastic limit of 6.7 GPa

(b) D, D^1 : theoretical Hugoniot, $\gamma = 1.57$

E, E^1 : actual Hugoniot, $\gamma = 1.57$, Hugoniot elastic limit of 6.7 GPa

Figure 13. Observed and theoretical temperatures for forsterite

(a) A, A^1 : polycrystalline forsterite, equilibrium Hugoniot

B, B^1 : $\sim$ 4% porous forsterite, equilibrium Hugoniot

C, C^1 : theoretical Hugoniot

(b) theoretical Hugoniot, $\gamma = 2.5$ on compression, 1 on release

E, E^1 : actual Hugoniot, assumed Hugoniot elastic limit 5 GPa

F : actual Hugoniot, elastic limit 9 GPa shock temperatures

Figure 14. Schematic diagram illustrating elasto-plastic release path.

Figure 15. Two release paths having the same initial slope and area underneath yet different final volumes.

Figure B-1 Static and dynamic streak images produced upon shock compression of c-cut single crystal forsterite to 17 GPa. (a) Static image as seen through streak camera. (b) Streak image demonstrating two-wave shock structure recorded by inclined mirror.

Figure B-2 Shock pressure versus density plot for forsterite showing the position of the Hugoniot elastic limit. The isentropic compression curve was calculated using a value of the bulk modulus and its pressure derivative of 128.8 GPa and 5.37 (see Table 9)

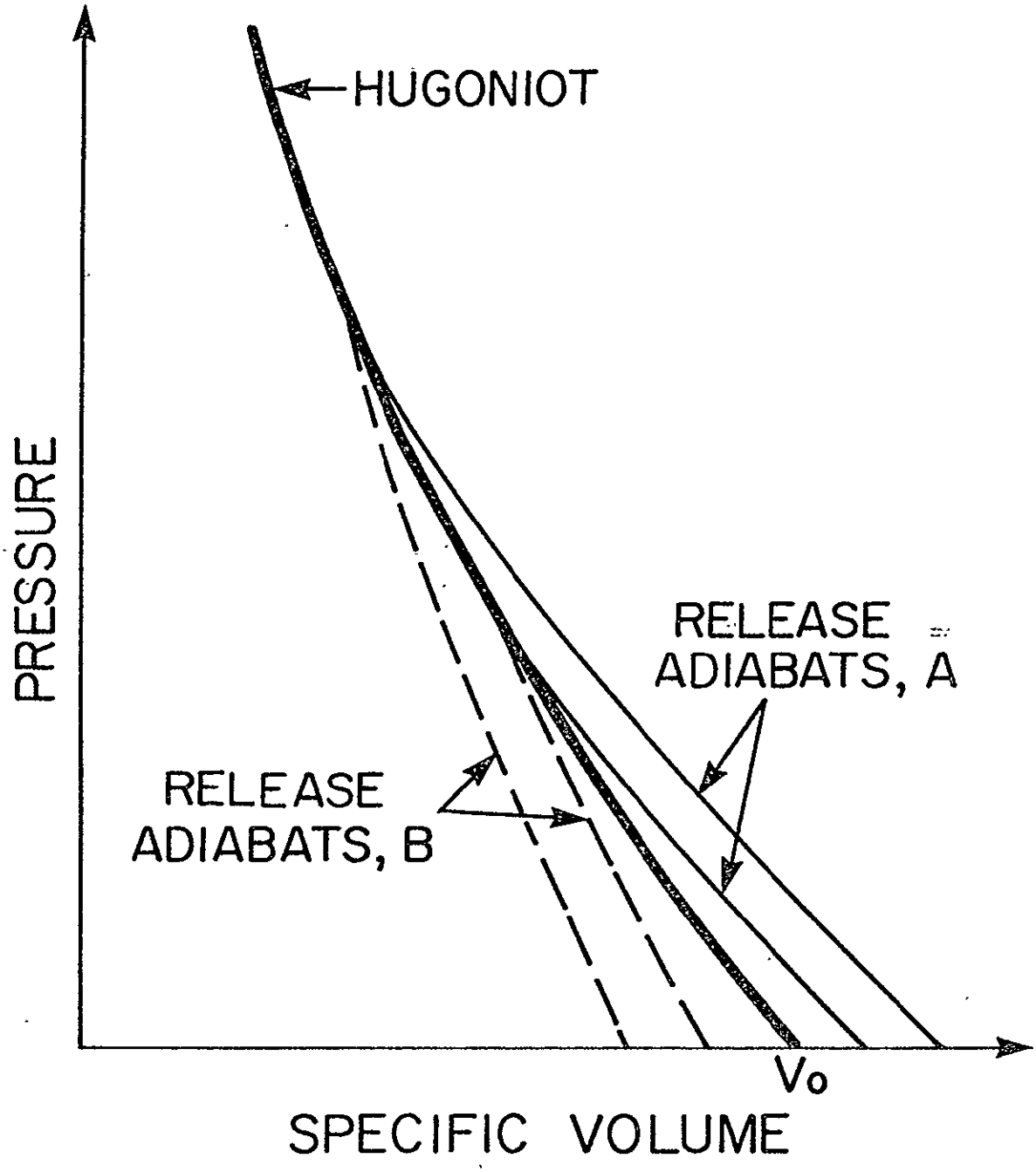
HUGONIOT
PRESSURE
RELEASE
ADIABATS, A
RELEASE
ADIABATS, B
Vo
SPECIFIC VOLUME

Fig. 1

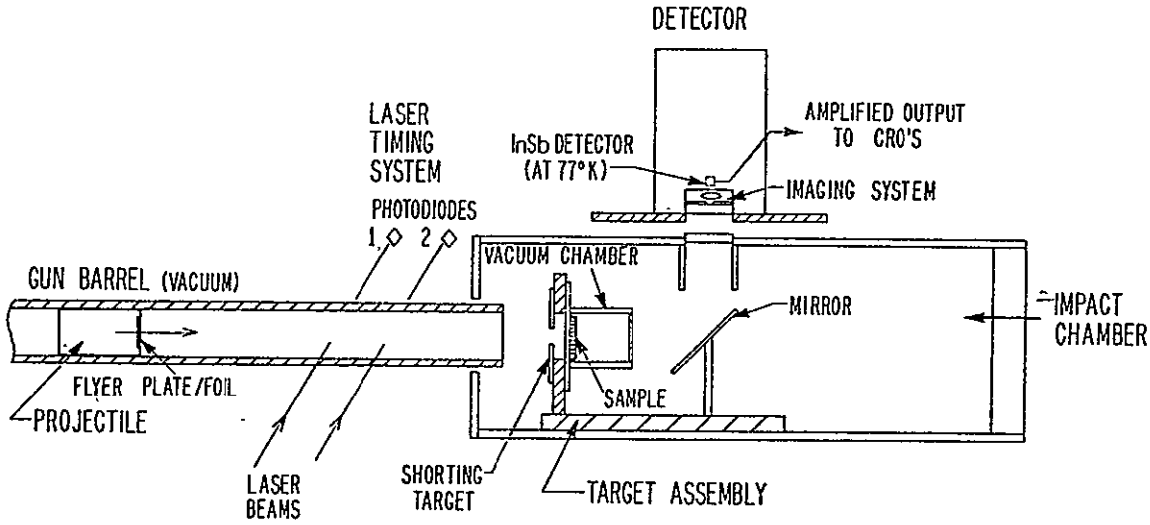
DETECTOR
LASER
TIMING
SYSTEM
InSb DETECTOR
(AT 77°K)
AMPLIFIED OUTPUT
TO CRO'S
IMAGING SYSTEM
PHOTODIODES
1
2
VACUUM CHAMBER
GUN BARREL (VACUUM)
MIRROR
IMPACT
CHAMBER
FLYER PLATE/FOIL
PROJECTILE
SAMPLE
LASER
BEAMS
SHORTING
TARGET
TARGET ASSEMBLY

Fig. 2

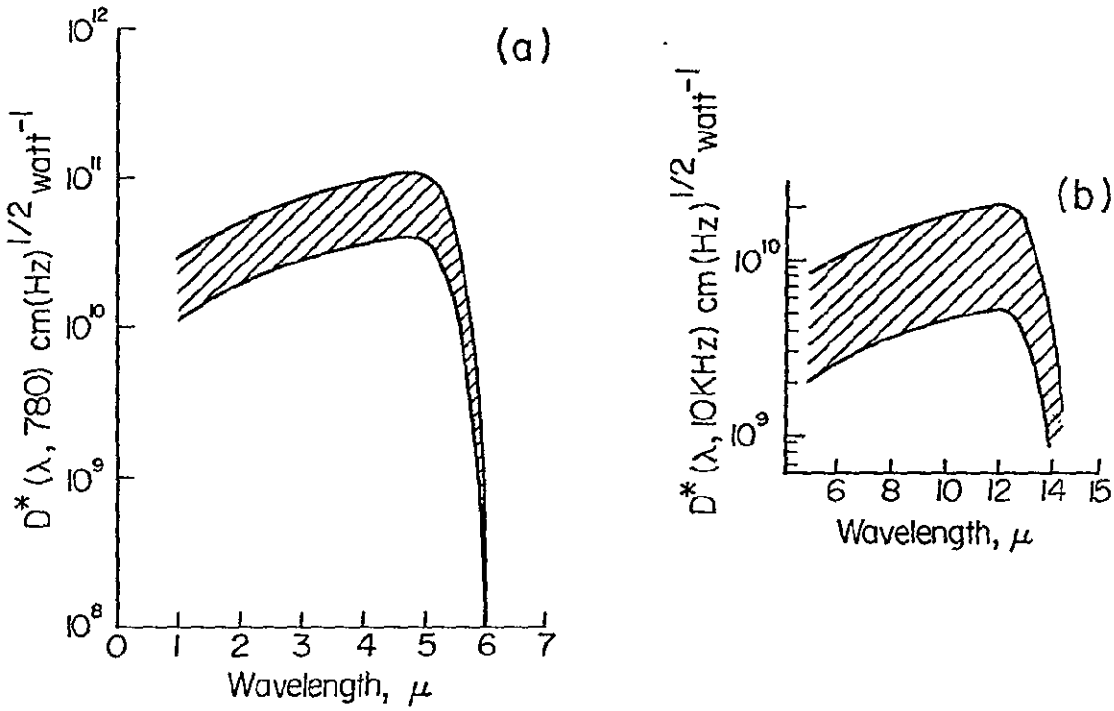
(a)
10^{12}
10^{11}
10^{10}
10^{9}
10^{8}
$D^*(\lambda, 780)$ cm(Hz)$^{1/2}$watt^{-1}
0 1 2 3 4 5 6 7
Wavelength, μ
(b)
10^{10}
10^{9}
$D^*(\lambda, 10KHz)$ cm(Hz)$^{1/2}$watt^{-1}
6 8 10 12 14 15
Wavelength, μ

Fig. 3

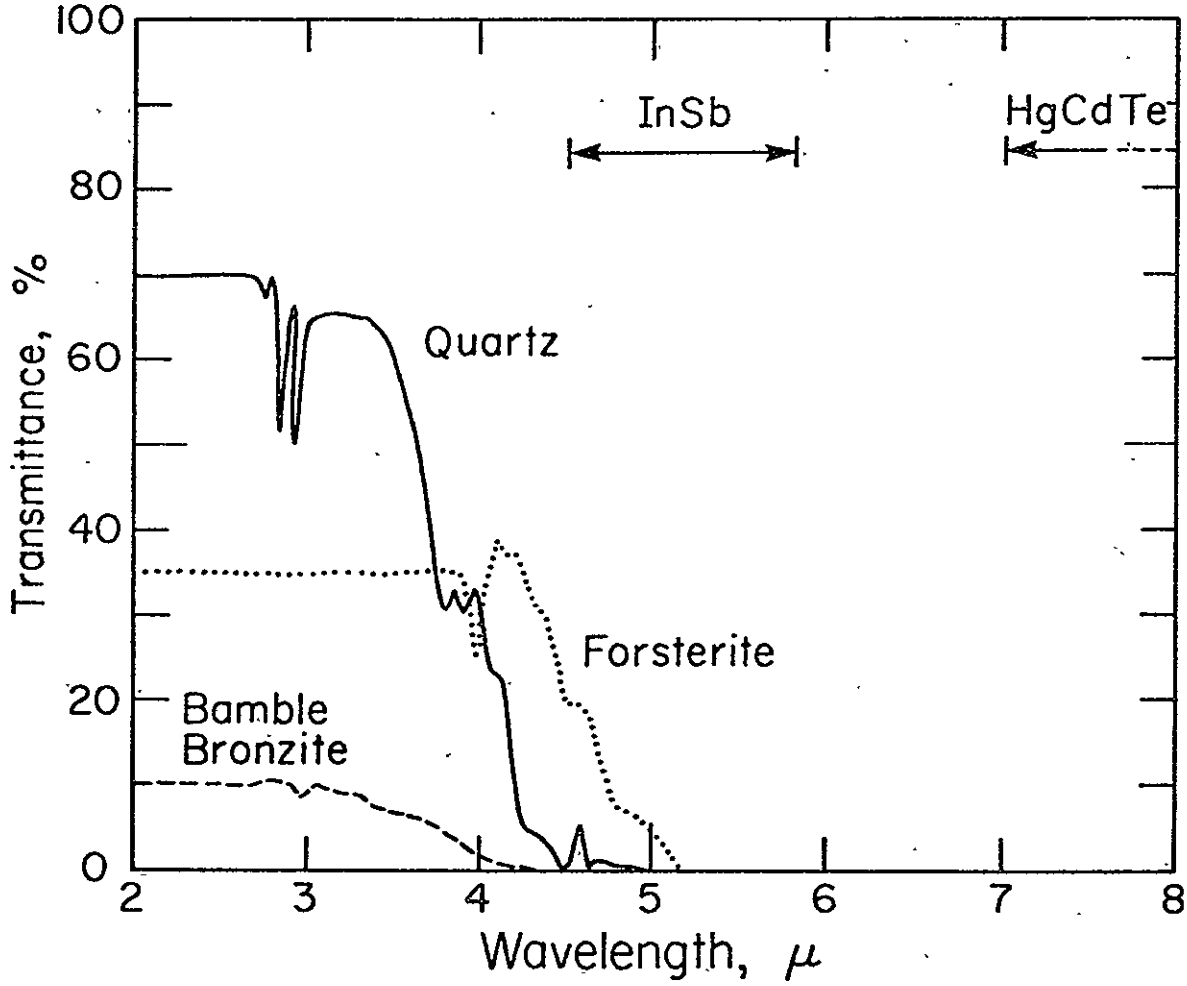
100
80
60
40
20
0
Transmittance, %
InSb
HgCdTe
Quartz
Forsterite
Bamble
Bronzite
2
3
4
5
6
7
8
Wavelength, μ

Fig. 4

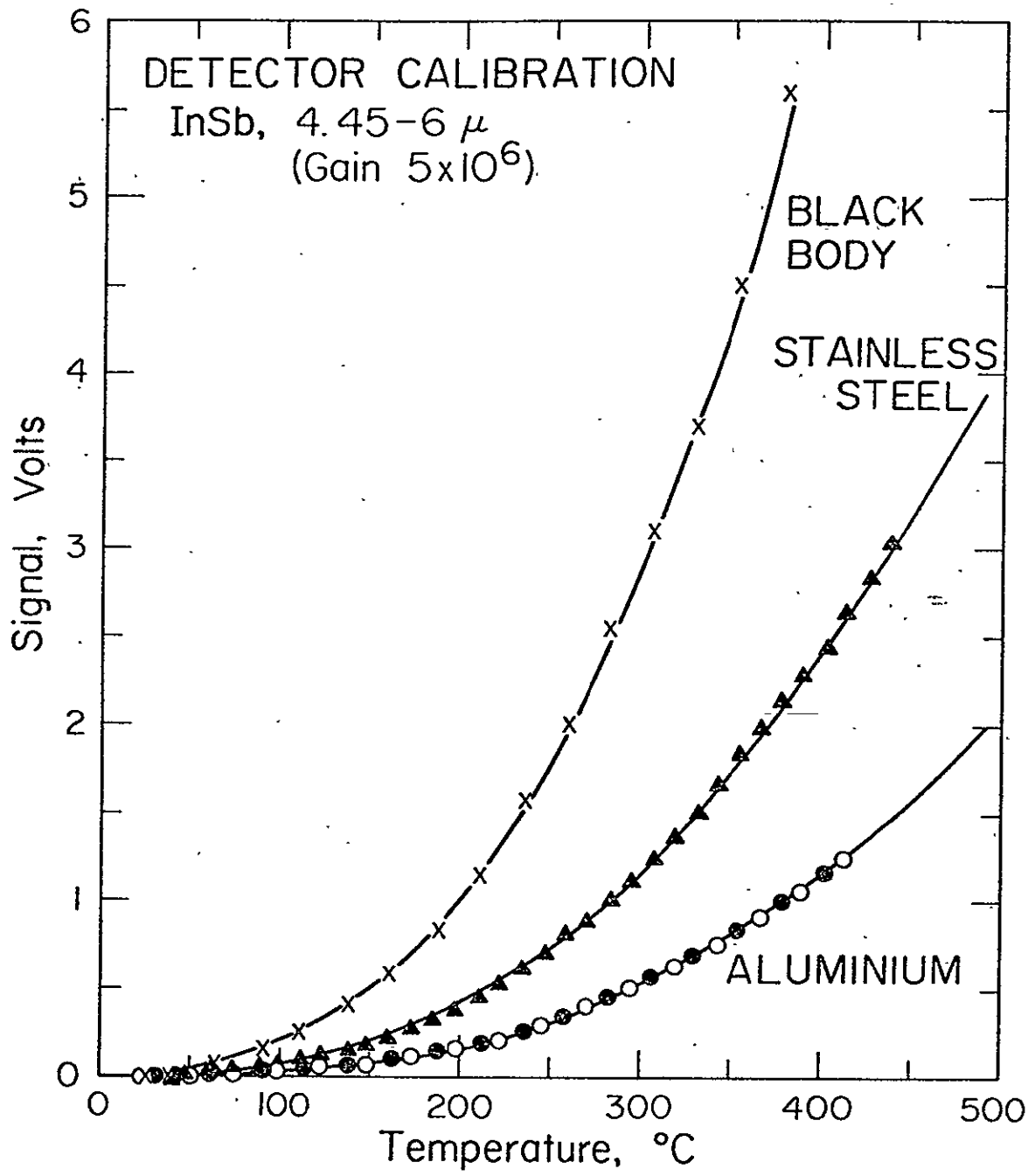
DETECTOR CALIBRATION
InSb, 4.45-6 μ
(Gain 5x10^6)
BLACK BODY
STAINLESS STEEL
ALUMINIUM
Signal, Volts
Temperature, °C
0
1
2
3
4
5
6
0
100
200
300
400
500

Fig. 5

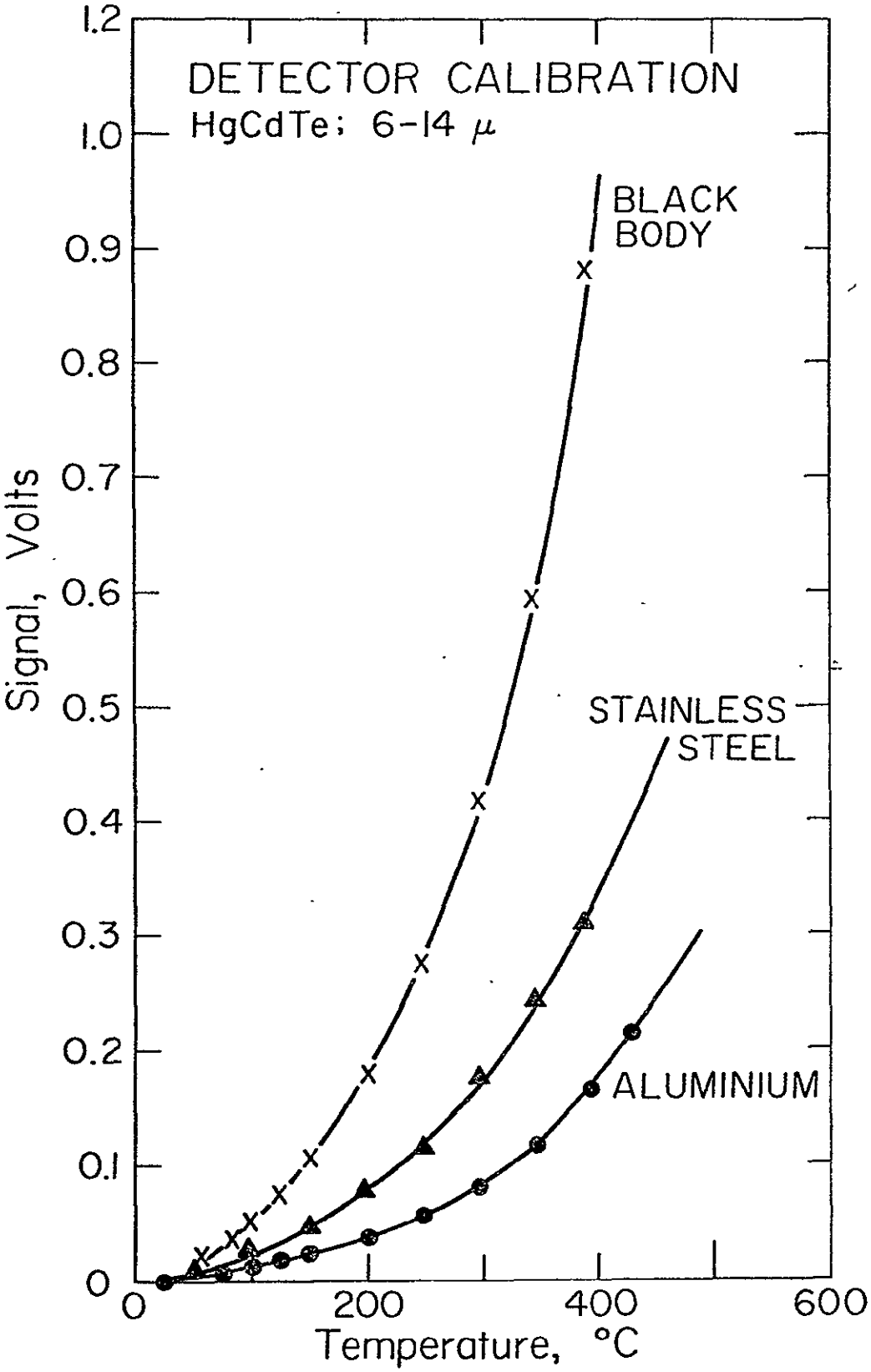
DETECTOR CALIBRATION
HgCdTe: 6-14 μ
BLACK BODY
STAINLESS STEEL
ALUMINIUM
Signal, Volts
Temperature, °C
0
0.1
0.2
0.3
0.4
0.5
0.6
0.7
0.8
0.9
1.0
1.2
0
200
400
600

Fig. 6

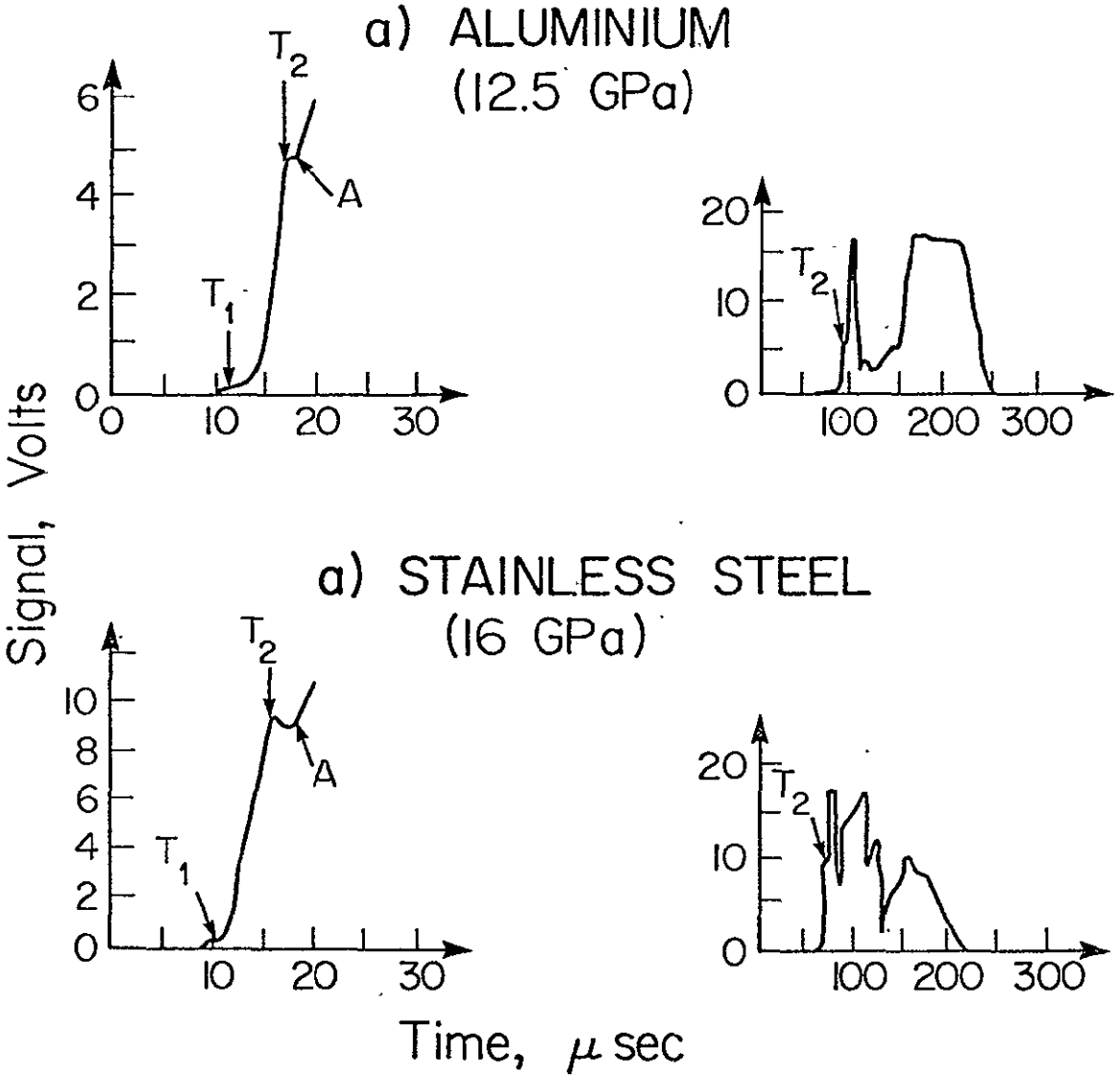
a) ALUMINIUM
(12.5 GPa)
a) STAINLESS STEEL
(16 GPa)
Signal, Volts
Time, μ sec
T1
T2
A
0
2
4
6
10
20
30
100
200
300

Fig. 7

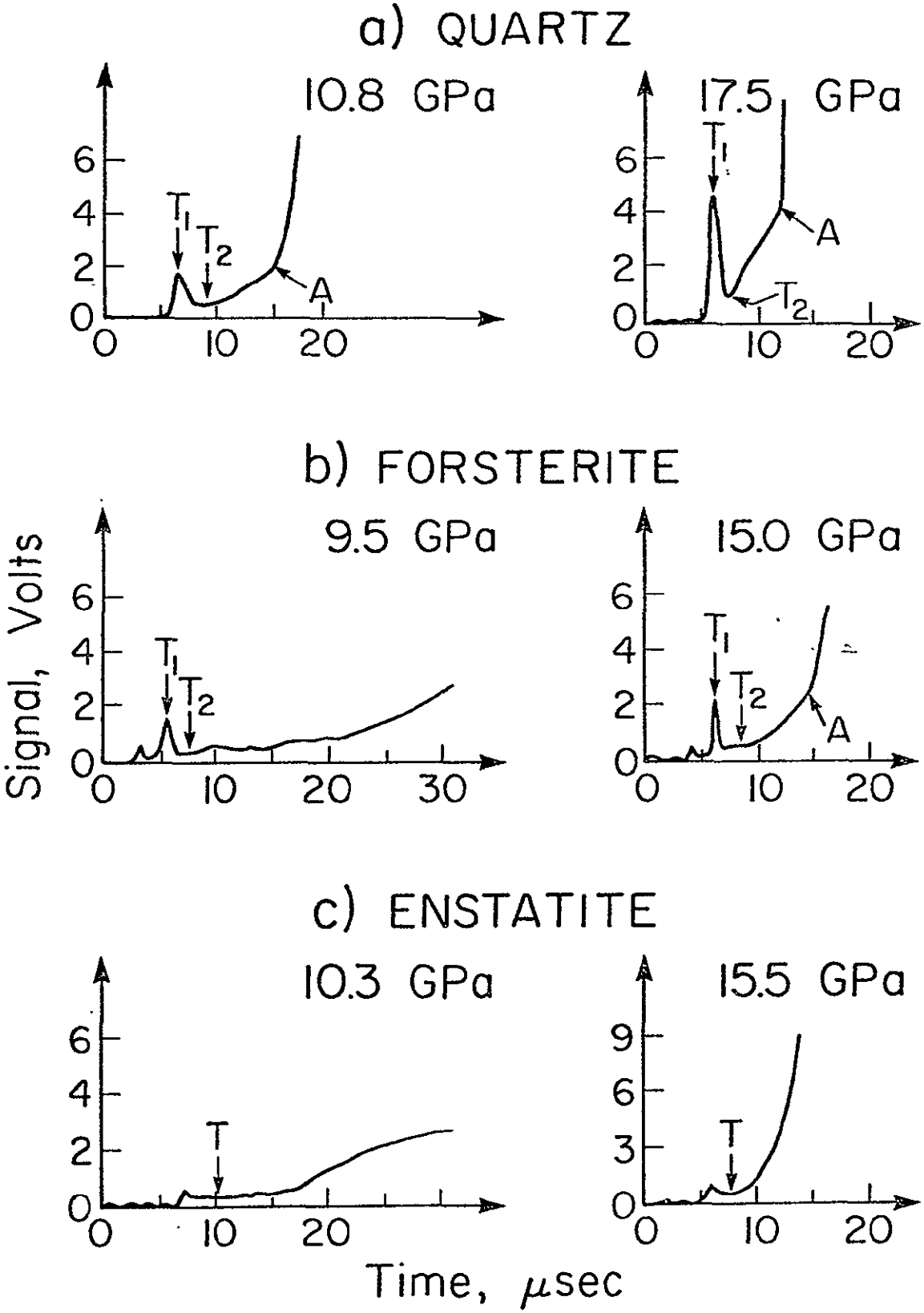
a) QUARTZ
10.8 GPa
17.5 GPa
b) FORSTERITE
9.5 GPa
15.0 GPa
c) ENSTATITE
10.3 GPa
15.5 GPa
Signal, Volts
Time, μsec
T1
T2
A
T

Fig. 8

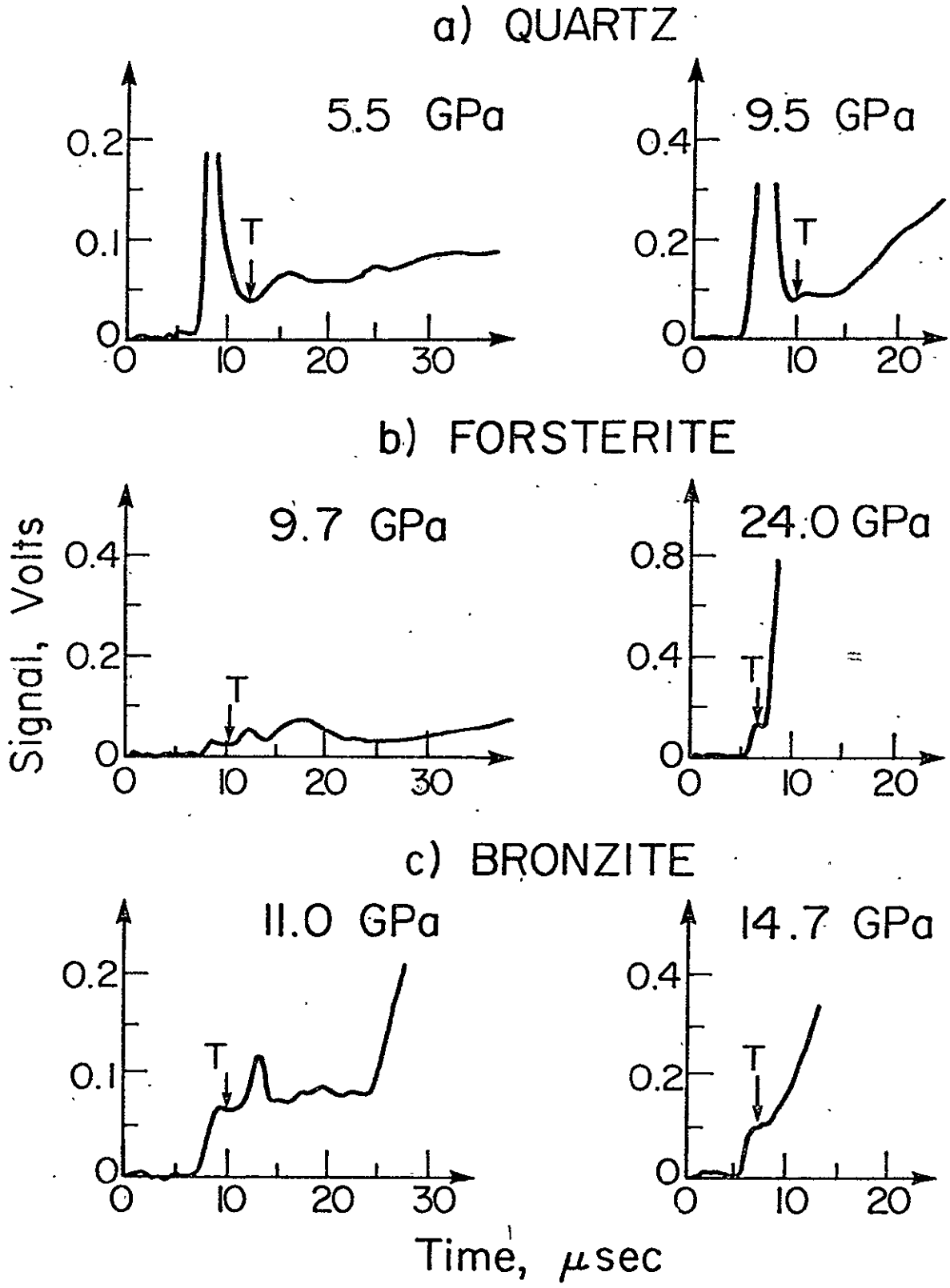
a) QUARTZ
5.5 GPa
9.5 GPa
b) FORSTERITE
9.7 GPa
24.0 GPa
c) BRONZITE
11.0 GPa
14.7 GPa
T
Signal, Volts
Time, μsec

Fig. 9

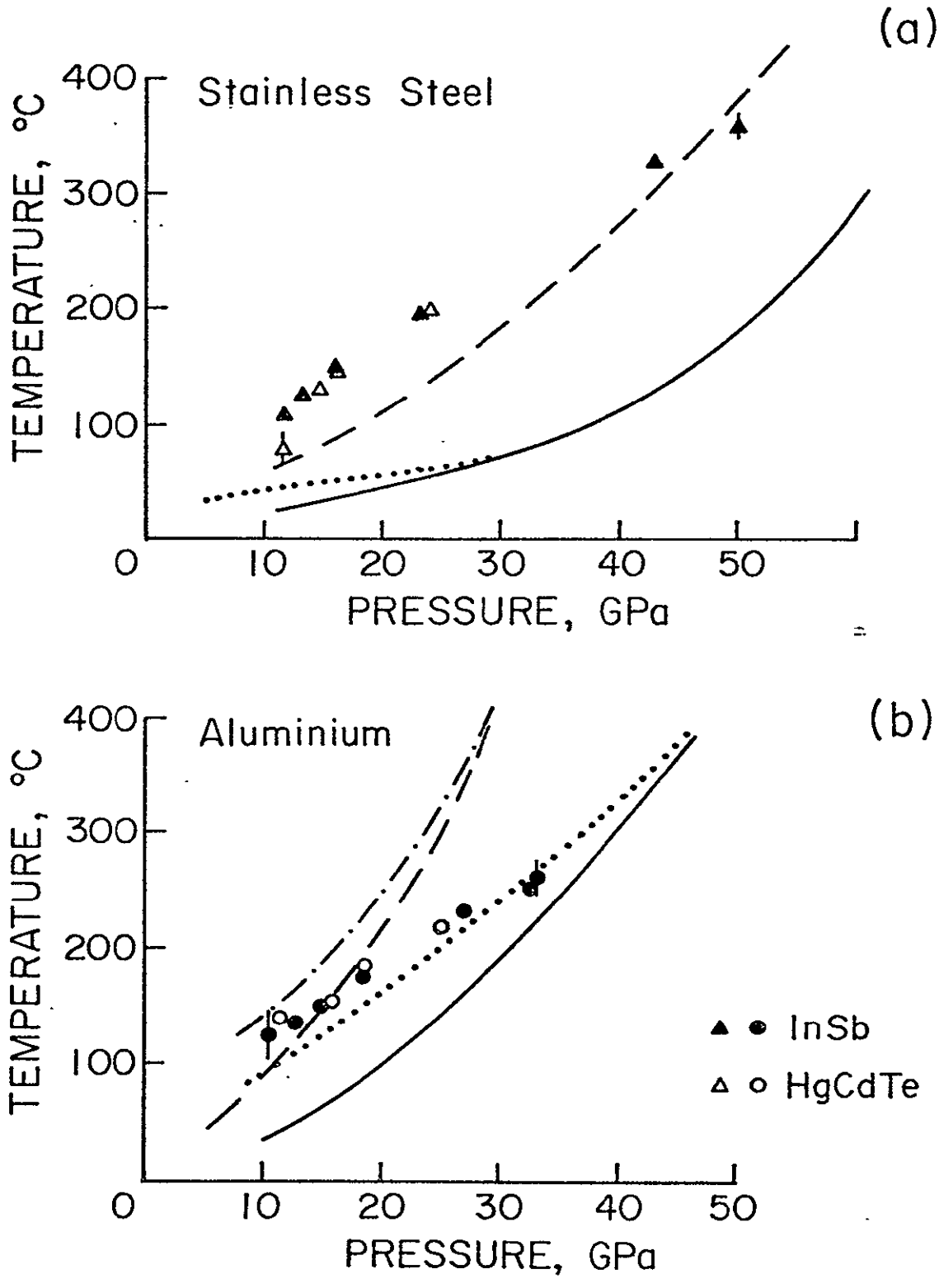
(a)
Stainless Steel
TEMPERATURE, °C
400
300
200
100
0
10
20
30
40
50
PRESSURE, GPa
(b)
Aluminium
TEMPERATURE, °C
400
300
200
100
0
10
20
30
40
50
PRESSURE, GPa
InSb
HgCdTe

Fig. 10

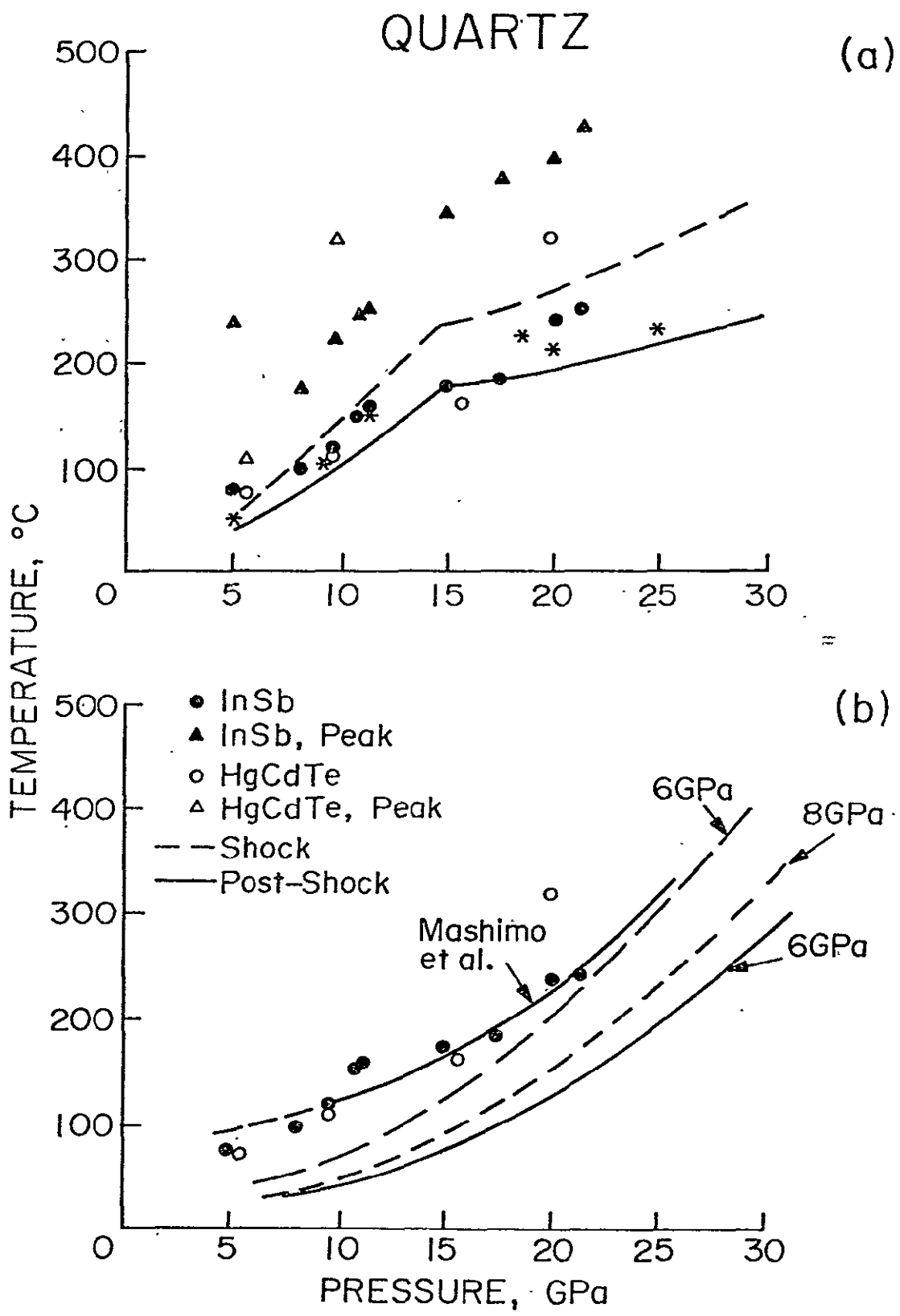
QUARTZ
(a)
500
400
300
200
100
0
5
10
15
20
25
30
TEMPERATURE, °C
(b)
InSb
InSb, Peak
HgCdTe
HgCdTe, Peak
Shock
Post-Shock
6GPa
8GPa
Mashimo et al.
6GPa
PRESSURE, GPa

Fig. 11

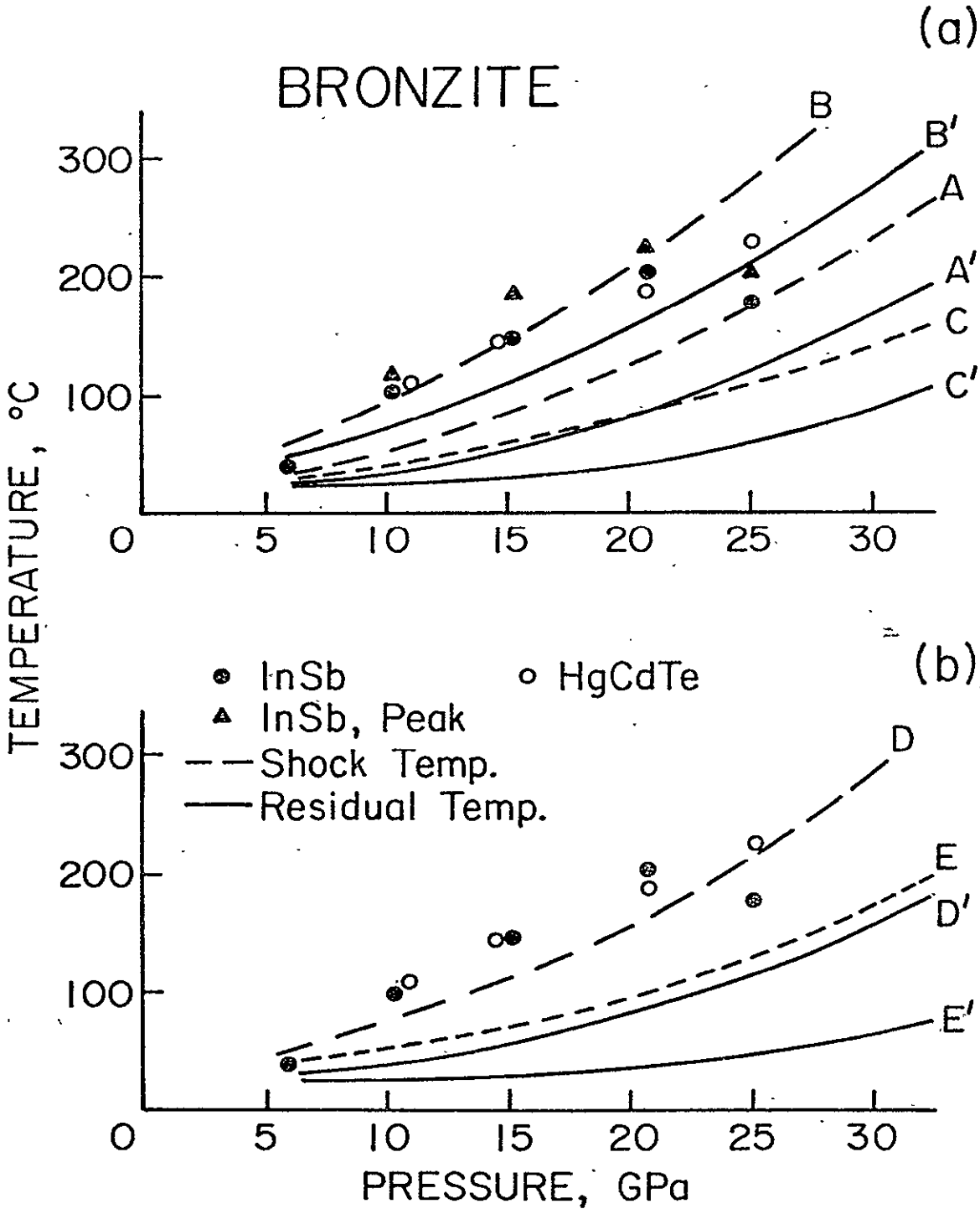
(a)
BRONZITE
B
B'
A
A'
C
C'
300
200
100
0
5
10
15
20
25
30
TEMPERATURE, °C
InSb
HgCdTe
InSb, Peak
Shock Temp.
Residual Temp.
(b)
D
E
D'
E'
PRESSURE, GPa

Fig. 12

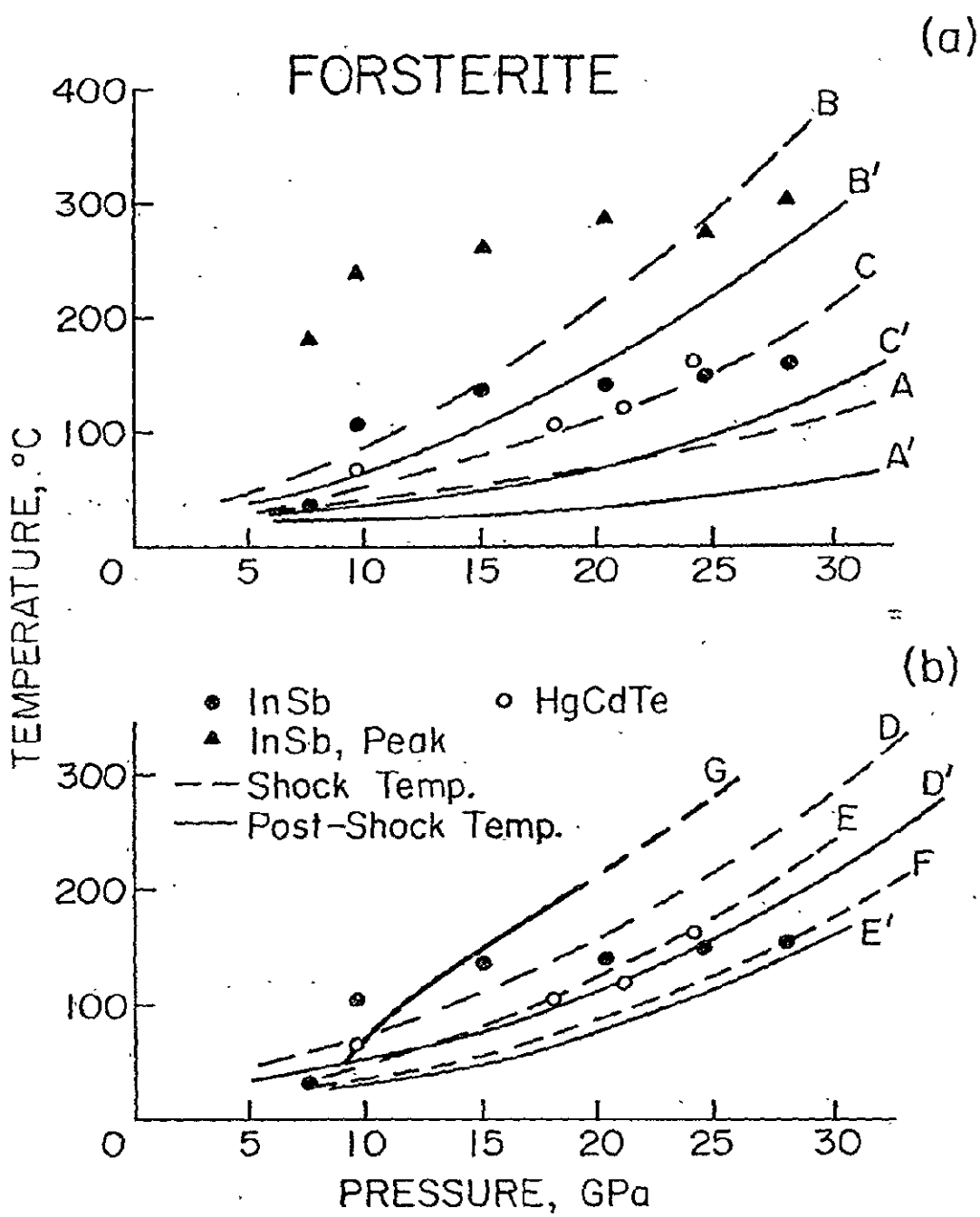
(a)
FORSTERITE
400
300
200
100
0
B
B'
C
C'
A
A'
5
10
15
20
25
30
(b)
InSb
HgCdTe
InSb, Peak
Shock Temp.
Post-Shock Temp.
TEMPERATURE, °C
PRESSURE, GPa
D
D'
G
E
F
E'

Fig. 13

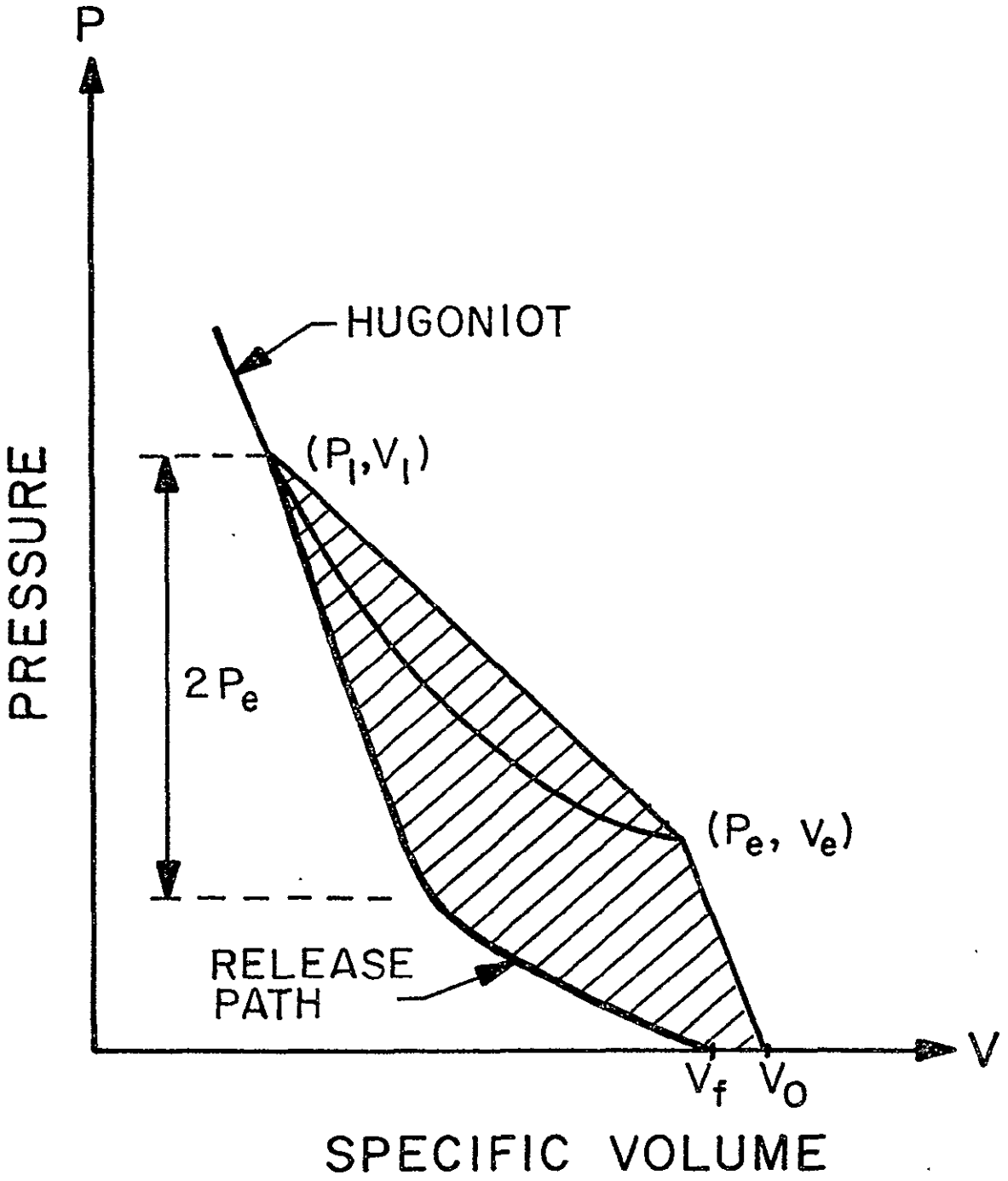
P
PRESSURE
HUGONIOT
(P_1, V_1)
$2P_e$
(P_e, V_e)
RELEASE
PATH
V
V_f
V_0
SPECIFIC VOLUME

Fig. 14

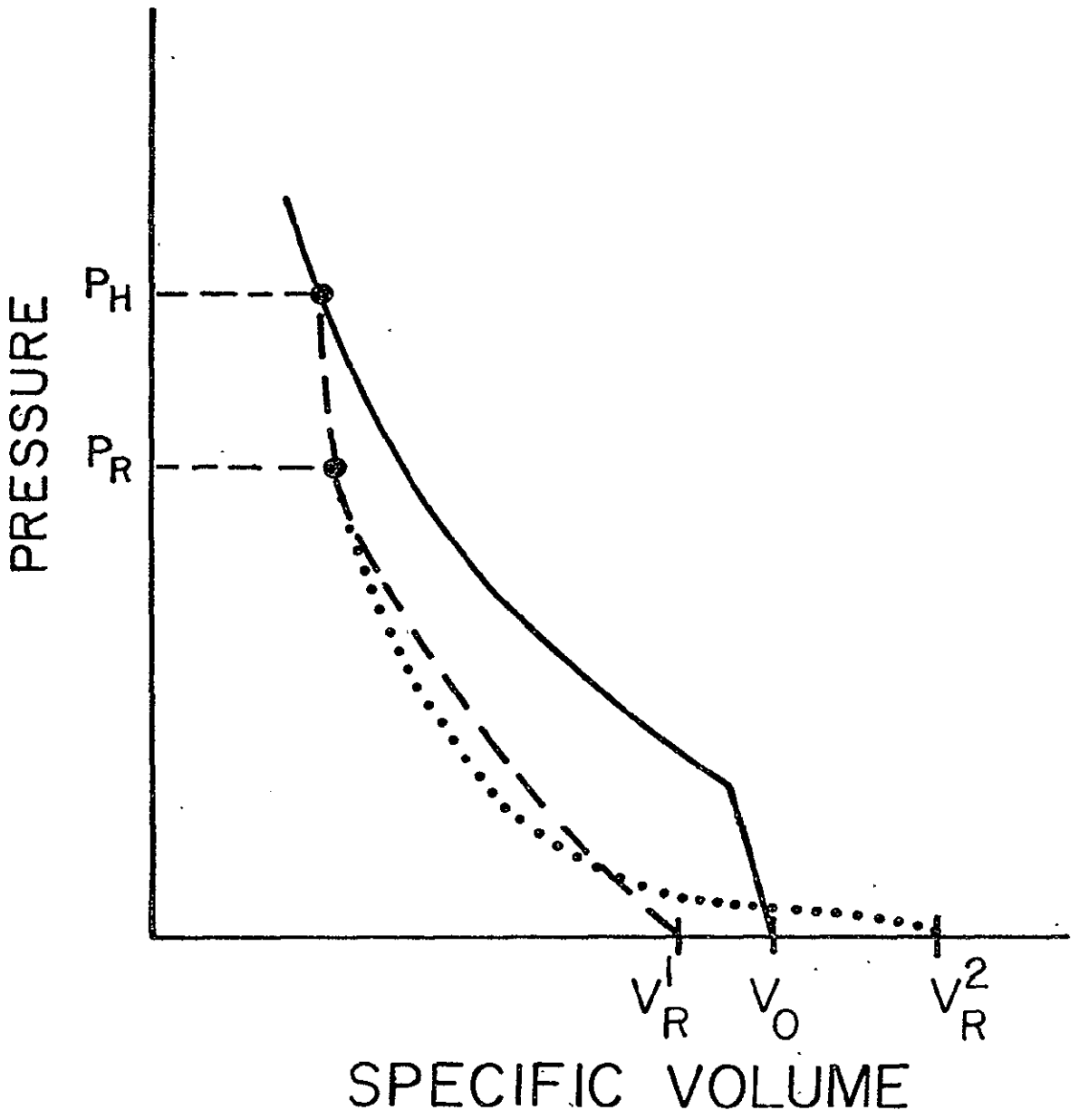

Fig. 15

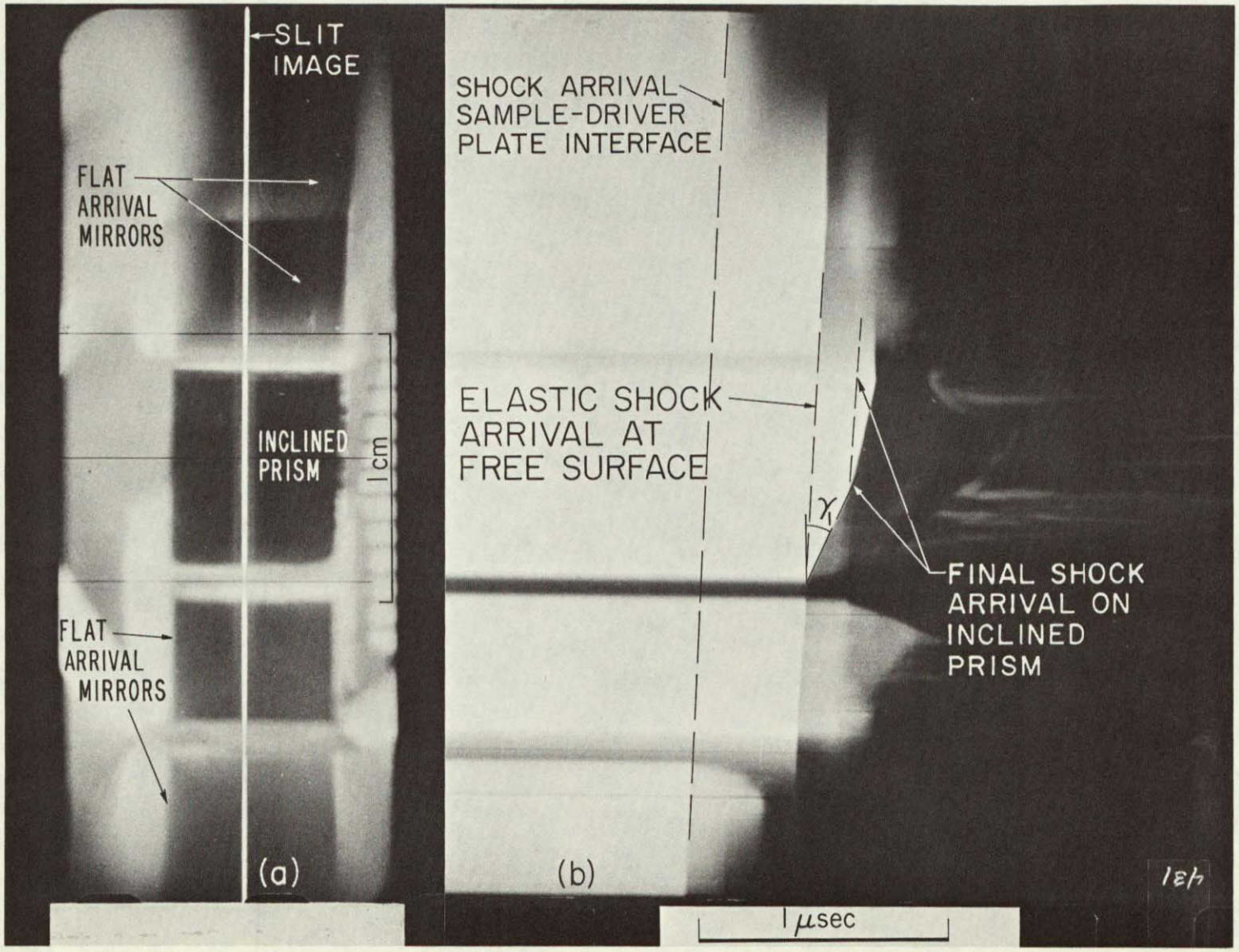

Fig. B-1

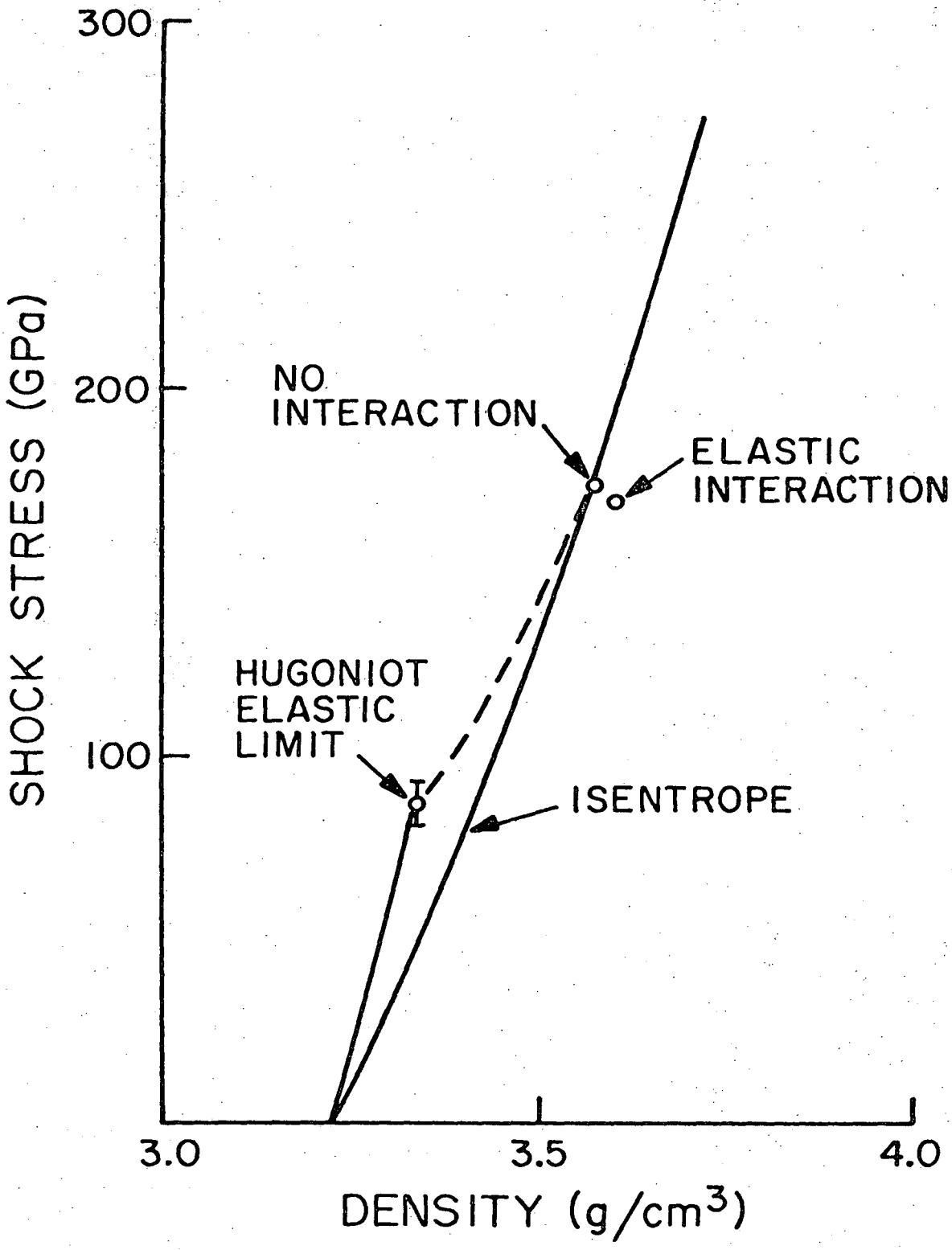
300
200
100
SHOCK STRESS (GPa)
NO
INTERACTION
ELASTIC
INTERACTION
HUGONIOT
ELASTIC
LIMIT
ISENTROPE
3.0
3.5
4.0
DENSITY (g/cm3)

Fig. B-2